Paleoceanographic Significance of Calcareous Nannofossil Assemblages in the Tropic Shale of Utah during Oceanic Anoxic Event 2 at the Cenomanian/Turonian Boundary

Victoria Fortiz[1, 2], Rosie Oakes[1, 3], F. Garrett Boudinot[4], Matthew M. Jones[5+], R. Mark Leckie[6], Amanda Parker[6], Bradley B. Sageman[5], Julio Sepúlveda[4] and Timothy J. Bralower[1*]

[1]*Department of Geosciences, Pennsylvania State University, University Park, PA 16802, USA*

[2] *Fugro, 13501 Katy Fwy Suite 1050, Houston, TX 77079, USA*

[3]*Meteorological Office, Exeter, Devon, UK*

[4]*Department of Geological Sciences and Institute of Arctic and Alpine Research (INSTAAR), University of Colorado, Boulder, CO 80309, USA*

[5]*Department of Earth and Planetary Sciences, Northwestern University, Evanston, IL 60208, USA*

(*[+]Current address: Geology, Energy & Minerals Science Center, United States Geological Survey, Reston, VA 20192, USA)*

[6]*Department of Geosciences, University of Massachusetts, Amherst, MA 01003, USA*

* corresponding author email: tjb26@psu.edu

ABSTRACT: Oceanic Anoxic Event 2 (OAE2) at the Cenomanian/Turonian Boundary (CTB: 93.9 Ma) involved the global deposition of organic carbon-rich sediments, a distinctive positive shift in carbon isotope values, and significant species turnover, including changes in calcareous nannofossil assemblages. While it is thought that volcanism triggered organic C-rich sediment deposition during OAE2, it is unclear whether enhanced productivity, increased stratification, of some combination of the two increased organic matter preservation. Calcareous nannofossil assemblages have the potential to qualitatively assess changes in ocean nutrient and temperature conditions to disentangle such ecological dynamics during OAE2. Here we study an expanded section of the Tropic Shale in a drill core in southern Utah near the western margin of the Western Interior Seaway (WIS) to understand how circulation changed during the event and how this may have influenced primary productivity and organic carbon burial. Relative abundance data of well-preserved nannoplankton are complemented with measurements of trace metal, and organic carbon and carbonate concentrations to determine changes in temperature and water column structure, as well as controls on surface water productivity. Detailed statistical analysis helps refine species paleoecologies combined with information from planktic and benthic foraminiferal assemblages and organic biomarkers. Changes in calcareous nannofossil assemblages indicate that near the start of OAE2 the western WIS surface ocean actually cooled for a short time. Following this, surface waters became warmer and more stratified as a Tethyan water mass invaded the seaway. Assemblages suggest that warmth persisted for much of the OAE2 interval, while stratification waxed and waned. The local seaway cooled near the end of OAE2 as Boreal water masses streamed along the western margin. Variations, including the decrease in the abundance of *Biscutum constans* and short-lived peaks in the abundance of *Eprolithus* spp. are super regional or possibly global in extent. There is no correlation between calcareous nannofossil assemblages and trace metal concentrations, suggesting they were unaffected by volcanism-related nutrient inputs. Assemblages support other data that suggest increased stratification influenced organic carbon burial in the Western Interior Seaway, and possibly elsewhere, during OAE2.

Keywords: Calcareous nannoplankton, Cenomanian-Turonian boundary, Oceanic Anoxic Event

INTRODUCTION

The Cenomanian/Turonian Boundary (CTB; 93.9 Ma) was characterized by an abrupt and short-lived carbon burial event (~600-800 kyr) (Sageman et al. 2006) known as Oceanic Anoxic Event 2 (OAE2) that corresponded to surface ocean warming of 7–8 °C (Forster et al. 2007), deep-water temperatures ~19 °C (Huber et al. 2002), pCO_2 ~3–7 times preindustrial levels (Damsté et al. 2008, Barclay et al. 2010), rapid spreading rates (Arthur et al. 1985; Larson 1991; Seton et al. 2009), and peak transgression (Kauffman 1977; Haq et al. 1987; Sageman et al. 1997; Gale et al. 2008). The climatic and biogeochemical perturbations at OAE2 are thought to have been triggered by extensive volcanism (Larson 1991; Leckie et al. 2002; Turgeon and Creaser 2008). Volcanic CO_2 input may have caused increased terrestrial weathering and nutrient input from rivers, leading to increases in primary production, and/or higher temperatures may have led to weakened ocean circulation that enhanced water column stratification, with both mechanisms causing decreased oxygen levels in ocean bottom waters (Schlanger and Jenkyns 1976; Arthur et al. 1987; Jenkyns 2010). These changes in water column properties are indicated by the deposition of organic C-rich sediments in a wide range of settings globally, from broad rises and plateaus in the Pacific, to the Tethyan continental margins, and the shallow shelf of northeastern Europe (Schlanger and Jenkyns 1976; Jenkyns 1980; Arthur et al. 1987; Arthur and Sageman 1994; Arthur and Sageman 2005; Jenkyns 2010; Robinson et al. 2017). OAE2 is characterized by a positive carbon isotope excursion (CIE), measured in bulk organic carbon ($\delta^{13}C_{org}$) and bulk carbonate ($\delta^{13}C_{carb}$), presumably as a result of the widespread burial of isotopically light carbon (Scholle and Arthur 1980; Jenkyns 2010; Robinson et al. 2017). The percent total organic carbon (TOC) is highly variable between sites (Pratt 1985; Schlanger et al. 1987; Dumitrescu and Brassell 2006).

The CTB is marked by a mass extinction event that included ammonites (93% extinction), semi-infaunal and boring bivalves (90% extinction), and gastropods (84% extinction) (Raup and Sepkoski 1982; Elder 1989; Harries and Little 1999). Calcareous nannoplankton turnover rates (origination and extinction) increased at the CTB (Watkins 1985; Bralower 1988; Leckie et al. 2002; Erba 2004). The relationship between extinctions, turnover of planktonic marine organisms, and ocean anoxia is not well understood. As indicated above, two possible mechanisms, alone or in concert, have been proposed to explain the deposition of organic C-rich sediments during OAE2: increased productivity and/or increased water-column stratification and preservation (Watkins 1989; Erba 2004; Arthur and Sageman 2005; Eleson and Bralower 2005; Meyers et al. 2005; Hardas and Mutterlose 2007; Mort et al. 2007; Turgeon and Creaser 2008; Elderbak and Leckie 2016). Increased productivity could have resulted from the rapid influx of micronutrients from hydrothermal activity associated with large submarine igneous province eruption, and increased seafloor spreading rates (Kerr 1998; Leckie et al. 2002; Erba 2004; Snow et al. 2005; Turgeon and Creaser 2008; Barclay et al. 2010). Alternatively, elevated productivity could have been caused by runoff of nutrients resulting from increased hydrologic cycling and continental weathering (Arthur et al. 1987; Arthur and Sageman 2005; van Helmond et al. 2014) and/or increased regeneration of phosphorus from organic-rich substrates (Meyers 2007; Mort et al. 2007; Adams et al. 2010). Increased water column stratification is a potential response to warming and changes in water density as the sources of surface waters shifted from Boreal to Tethyan during OAE2 (Burns and Bralower 1998; Leckie et al. 1998; Erba 2004; Eleson and Bralower 2005; Hardas and Mutterlose 2007; Corbett and Watkins 2013; Elderbak and Leckie 2016). While these two mechanisms have each been proposed, more comprehensive multi-proxy ecological comparisons are required to disentangle their relative roles during OAE2.

The Tropic Shale was deposited near the western edge of the Western Interior Seaway (WIS) during the latest Cenomanian and early Turonian. The epicontinental seaway connected polar Boreal and subtropical Tethyan waters. Freshwater influx to the seaway came from the Sevier Highlands to the west, the Mogollon Highlands to the southwest, and from the stable craton to the east. The WIS was heavily influenced by regional changes in water mass stratification and mixing, increased productivity due to fluvial input of nutrients, changes in relative sea level and ocean circulation, benthic ventilation, and changes in dominant surface water mass from both Tethyan and Boreal sources (Schlanger and Jenkyns 1976; Arthur et al. 1987; Leckie et al. 1998; Lowery et al. 2018; Jones et al. 2019; Boudinot et al. 2020).

Calcareous nannofossil assemblages during OAE2 in the WIS are marked by large shifts between taxa with eutrophic and oligotrophic affinities (Watkins 1986; Watkins 1989; Watkins 1993; Burns and Bralower 1998; Eleson and Bralower 2005; Corbett and Watkins 2013; Lowery et al. 2014; Lowery et al. 2018). Assemblages have the potential to be used to qualitatively assess changes in nutrient and surface-ocean temperature conditions using known paleoecological affinities of taxa (Thierstein 1981; Roth and Krumbach 1986; Roth 1989; Silvá et al. 1989; Watkins 1989; Erba et al. 1992; Mutterlose and Kessels 2000; Hardas et al. 2012; Herrle et al. 2003; Bottini and Erba 2018; Tiraboschi et al. 2009; Faucher et al. 2017).

The western edge of the WIS is an ideal location for reconstructing such change in nutrient and surface ocean temperature conditions as fossil preservation in the Tropic Shale is excellent and depositional rates were high, allowing for high temporal resolution. This study of a continuous core of the Tropic Shale recovered along the western seaway margin (Jones et al. 2019; Boudinot et al. 2020) addresses the response of calcareous nanoplankton assemblages to the oceanographic perturbations that occurred during OAE2. Our investigation of assemblages is coupled with analyses of percent $CaCO_3$ and TOC, and trace metal concentrations to assess the timing and nature of volcanism (Orth et al. 1993; Snow et al. 2005; Faucher et al. 2017). In particular, we investigated the following questions: 1) What was the response of calcareous nannoplankton assemblages to environmental perturbations during OAE2 in the western prodeltaic shoreline of the WIS? (2) What were the mechanisms that controlled shifts in nannofossil assemblages? (3) Is there a correlation between calcareous nannofossil assemblages, $CaCO_3$, TOC, and trace metal concentrations that provides information about the mechanisms controlling organic carbon burial? (4) Finally, what was the nature of water mass and nutrient influx changes suggested by calcareous nannofossil assemblages? Our goal is to compare this information with evidence from foraminiferal studies and biomarkers (Boudinot et al. 2020) to aid in the interpretation of changes in ocean circulation, stratification, and productivity. Understanding abiotic and biotic interactions during this time of environmental change in a high CO_2 world has significant potential to inform possible future responses to anthropogenically induced climate and environmental change, including hypoxia in coastal environments.

MATERIAL and METHODS

Materials

The Smoky Hollow corehole recovered in July 2014 is located within the Grand Staircase-Escalante National Monument on the Kaiparowits Plateau near Big Water, south central Utah (37.158466°; -111.531947°; text-fig. 1). At this location, the Tropic Shale is ~120-m thick and consists of rhythmically-bedded dark gray, laminated to burrowed, silty to calcareous shale, sandy mudstone and carbonate-rich layers. These cycles likely represent Milankovitch-style orbital forcing of climate that influenced sedimentation sufficiently to overprint the effect of tectonically-induced variations in foreland basin subsidence (Elder et al. 1994; Uličný 1999; Laurin and Sageman 2007; Meyers et al. 2012; Jones et al. 2019; Laurin et al. 2019). The Tropic Shale was deposited in a prodeltaic environment within ~150 km of the western margin of the WIS (Leithold 1993) and overlies the Naturita Formation, a highly bioturbated marginal marine facies (Young 1960; Uličný 1999; Carpenter et al. 2014; McKean and Gillette 2015). In southern Utah there is a robust record of relative sea level changes preserved in the interfingering of the Tropic Shale with the Naturita and overlying Straight Cliffs Formation. Leithold (1994) identified six depositional sequences in the Tropic Shale corresponding to the long-term transgressive-regressive Greenhorn Cycle (Leithold 1994). Elder et al. (1994) focused on the parasequence scale packages of the Cenomanian to lowermost Turonian part of the succession and concluded that Milankovitch climatic forcing of sediment supply modulated the transgressive-regressive packages, with transgressive lags correlating basinward into limestone beds that are traceable across Colorado and Kansas. Later investigations by (Jones et al. 2019; Laurin et al. 2019; Jones et al. 2021) have provided support for these interpretations.

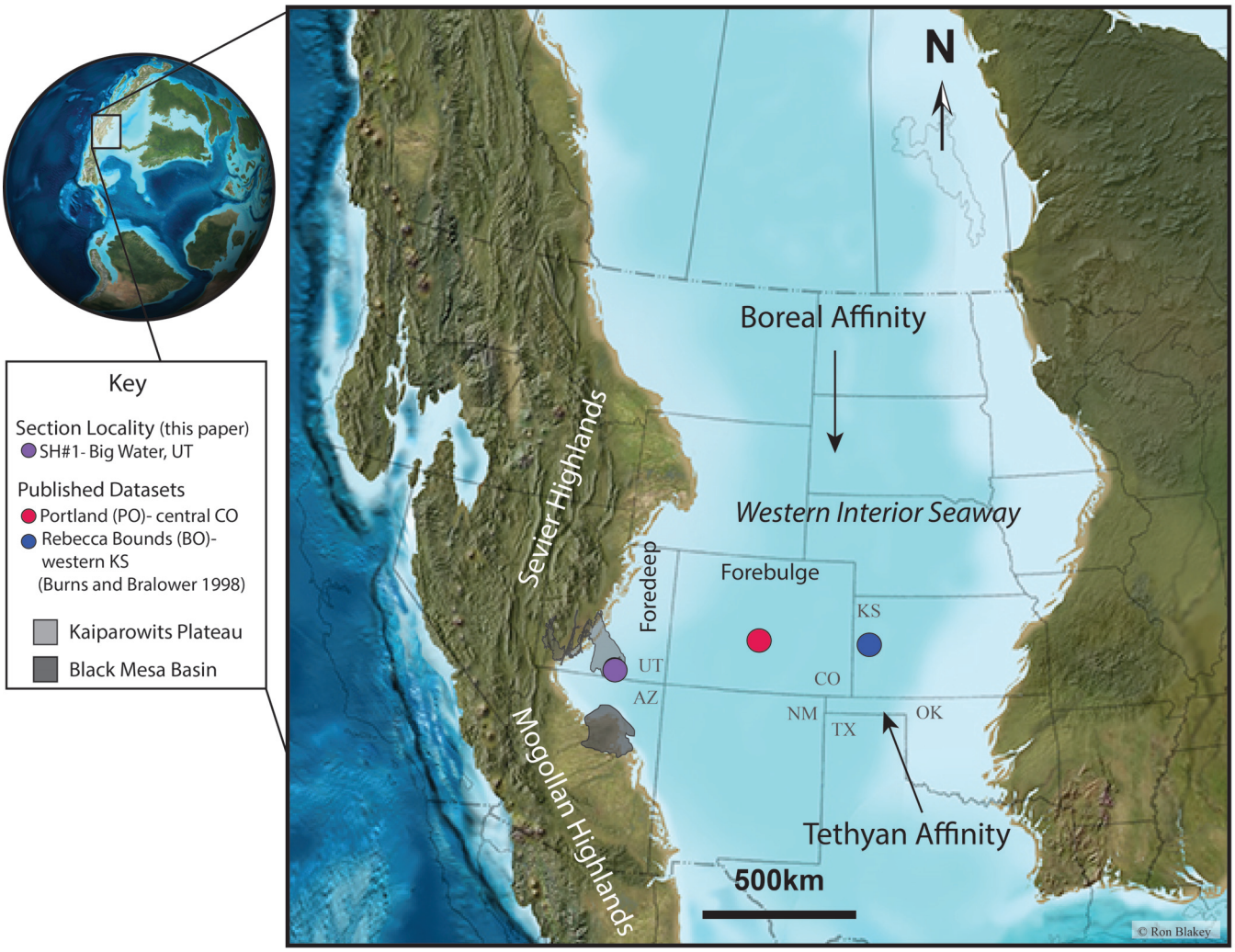

TEXT-FIGURE 1
Late Cretaceous paleogeographic reconstruction of the Western Interior Seaway (Ziegler et al. 1987; McCabe and Parrish 1992). Shown are present day locations of the Kaiparowitz Plateau (south-central Utah) and Black Mesa Basin (northeastern Arizona), as well as location of SH#1 core (this study), Portland core (near Pueblo, Colorado), and Rebecca Bounds core (western Kansas). To the west of the shoreline, the Sevier and Mogollan Highlands provided freshwater influx. To the east, a relatively shallow seaway extended from Alaska to Mexico connecting the Boreal Sea and Tethys Ocean (Kauffman 1984; Kauffman 1977).

The Smoky Hollow core (SH#1) is comprised of a ~30-m (100 ft.) thick section including the top of the Naturita Formation (upper Cenomanian) and the lower part of the Tropic Shale (uppermost Cenomanian–lower Turonian) (text-fig. 2). Lithology and carbon isotope stratigraphy are described in Jones et al. (2019). A fresh outcrop section nearby was also measured and described (Jones et al. 2019). The Tropic Shale can be correlated with age equivalent strata across the WIS using several significant bentonite layers (A1, A2, B, C, and D) along with limestone beds LS1 to LS10 (text-fig. 2) (e.g., (Kauffman 1977; Elder 1985; Elder et al. 1994; Meyers et al. 2012; Jones et al. 2019; Jones et al. 2021). This interval is characterized by the late Cenomanian and early Turonian *Metoicoceras mosbyense*, *Sciponoceras gracile, Neocardioceras juddii* and *Watinoceras devonense* ammonite biozones (Elder et al. 1994; Tibert et al. 2003).

Calcareous nannoplankton biostratigraphy and assemblage analysis

One hundred fifty-five samples from the Tropic Shale were studied for calcareous nannoplankton biostratigraphy and assemblage studies. Most samples disaggregated in water and a few lithified samples were broken apart using a mortar and pestle (Monechi and Thierstein 1985). For biostratigraphy, thick slides were prepared so that rare specimens could be detected. Nannofossils were identified based on the taxonomy of (Perch-Nielsen et al. 1985) and Nannotax (www.mikrotx.org/Nannotax3/). Slides were observed for approximately 30 minutes in a Zeiss Axio Imager A2 photomicroscope at a magnification of 1250x. We paid special attention to the identification of marker taxa. Preliminary biostratigraphic results were reported in Jones et al. (2019), but detailed data and documentation are presented

TABLE 1
Nannofossil biostratigraphy of the Smoky Hollow Core (SH #1). Taxa in yellow are the those that have been counted in the assemblage work.

sample	ABUNDANCE	PRESERVATION	Axopodorhabdus albianus	Biscutum constans	Broinsonia enormis	Broinsonia signata	Chiastozygus litterarius	Chiastozygus spp.	Corollithion achylosum	Corollithion signum	Cretarhabdus angustiforatus	Cretarhabdus conicus	Cretarhabdus coronadventis	Cretarhabdus loriei	Cretarhabdus surirellus	Cribrosphaerella ehrenbergii	Cyclagelosphaera margerelii	Eiffellithus turriseiffelii	Eprolithus floralis	Eprolithus moratus	Flabellites oblongus	Gartnerago segmentatum	Grantarhabdus coronadventis	Helenea chiastia	Helicolithus trabeculatus	Lithraphidites carniolensis	Manivitella pemmatoidea	Markalius circumradiatus	Microrhabdulus decoratus	Prediscosphaera cretacea	Prediscosphaera spinosa	Quadrum gartneri	Radiolithus planus	Rhagodiscus achlyostaurion	Rhagodiscus angustus	Rhagodiscus asper	Rhagodiscus splendens	Rotelapillus laffittei	Scapholithus fossilis	Sollasites horticus	Tetrapodorhabdus decorus	Tranolithus gabalus	Tranolithus orionatus	Vagalapilla octoradiata	Vagalapilla sp.	Watznaueria barnesiae	Watznaueria ovata	Zeughrabdotus embergeri	Zeughrabdotus diplogrammus	Zeughrabdotus elegans	Zeughrabdotus spiralis	Zeughrabdotus erectus
100.29 A	M			R	R	R	R					R			R			R	R	R		R			R					R	R	R												R	C		R	R	
100.9 C	M			R	R	R		R	R	R					R	R		R	R	R			R		R					R	R	R												R	F	R		R	R	
101.69 C	M			R	R	R		R			R	R			R			R	R	R					R					R			R		R									R	C		R	R	R
102.5 C	M			R		R		R		R	R				R			F				R			R		R		R				R											A		R	R	R	R
103.6 C	M			R		R						R			R			R	R	R					R			R		R	R	R			R									C		R	R	R	R
104.5 C	M			F		R				R		R			R			R	R	R		R			R					R			R											C		R	R	R	R
104.7 C	P			F		R				R	R				R			R	R	R		R			R					R			R											C	R		R		R
105.1 A	M			C		R				R	R				R			R				R			R	R	R			R			R	R											A		R	R	R	R
105.89 C	P			R		R				R				R	R			R	R	R					R					R			R	R											C		R	R	R	R
106.7 A	P		R	R	R	R									R			R	R	R					R					R				F			R								A			R	R	R
107.5 A	M		R		R	R							R		R		R	R	R	R					R					R	R		R											C		R	R	R	
108.52 A	M		R		R	R		R							R			R	R	R					R		R			R	R				R									A		R	R	R	
109.1 A	M		R	R	R		R			R					R			R	F	R					R		R			R			R	R											C		R	R	R	
110.1 C	P		R		R										R			R	R	R					R					R															F		R	R		
111.28 F	P		R	R	R										R			R	R	R					R					R															F		R	R		
112.7 A	M		R	R	R										R		R	R	R	R			R		R	R	R			R			R		R						R	R	C		R	R	R	
113.69 A	M		R		R		R		R	R					R			F	F	R	R				R		R			F			R	R	R		R						R	C	R		F	F	
114.2 A	M		F	R	R		R				R				R	F	R	R	R	R		R	R		R					R			R		R									R	C		R	R	R	R
114.89 A	M		R	R	R	R	R						R		R		R	R	R	R	R	R			R					R	R		R		R									R	A		R	F		
115.495 A	M		R		R	R					R				R			R	R	R					R					R	R			R									R	A		R	R	R	
115.885 A	M		R		R	R					R				R			R	R	R		R			R					R	R		R		R		R						R	A		R	R	R	
116.49 A	M		R		R	R									R			R	R	R	R	R			R		R			R			R		R		R						R	C	R	R	A		R	R	R	
117.09 C	M		R	R	R	R		R					R		R		R	R	R	R					R					R			R	R	R		R						R			C		R	R	R	
117.49 A	M		R		R	R					R				R		R	R	R	R		R	R	R	F					F	R			R	R	R						R	R		A		R	R	R	
118.1 A	M		R		F			R		R					F			F	R	R		R		R	F					R	R			R	R	R						F	R	R	A		R	R		
118.3 C	M		R		F	R					R				R			R	R	R	R	R			F					R				R		R						C	R		C	R		R	F		
118.6 A	M		R		C	R					R				R			R	R	R	R	R			F					R				R	R	R						F	R		C		R	R	R	
118.8 C	M	R	R		F	F									R			R	R	R		R			F					R				R									F	R		C		R	R		
119 A	M		R		C				R		R				R		R	F	R	R	R	R		R	F					R				R	R	R						R	R		A	R		R	R	R	
119.445 C	M	R	R		C										R			F	R	R		R		R	F					R				R	R	R						F	R	R	A	R		R	R	R	
119.7 C	M		R	R	R		R								R			F	R	R					R					R				R							F	R		C		F	R			
119.95 C	M		R		R										R			R	R	R		R			R					R				R									R		C	R		R	F	R	
120.205 C	M		F		F										F			F	R	R					R	R				F				R						R			F	R		C		F	F		
120.25 A	M		F		R	R									R			R	R	R		R			R	F	R	R		R				R									F	R	R	A		F	F	R	
120.45 A	M		R	R	R	R	R	R		R	R				R	R		F	R	R		R		R	R		R		R	R				R	R	R					R	R	R	A		R	F	F	R
120.85 A	M	R			R	R		R		R	R				R			F	R			R		R	R	R			R	R		R							R			R	A		F	F	C	
121.35 A	P	R	R		R	R		R			R				R			R	C	R					R					R	R			R			R						R	A		R	R	R	
121.8 A	M	R	R		R										R		R	R	F	R					R		R		R	R	R						R						F		R	A		R	R	R	
122.09 A	M	R	R	R	R	R					R				R		R	R	C	R				R	R		R			R	R				R			R						F			A		R	F	R	
122.32 C	P	R	R		R					R					R			R	R	R					R					R	R			R	R									R		R	C	R	R	R	R	R

A-Abundant (>10 sepcimens per field of view)
C-Common (1-10 sepcimens per field of view)
F-Few (>1 sepcimens per 10 fields of view)
R-Rare (<1 sepcimens per 10 fields of view)

herein (Table 1). The marker taxa, *Axopodorhabdus albianus* and *Helenea chiastia* are very rare near the end of their ranges, however, slides are thick and specimens are well preserved, thus we believe that the datums are precise. The marker *Quadrum gartneri* is exceedingly rare and occurs sporadically as in most sections near the beginning of its range, thus we feel less confident about this datum.

For assemblage studies, sampling resolution is the highest around the onset of OAE2 and decreases upcore. Additional sampling was done to constrain peaks in nannofossil assemblage counts. The resolution fluctuates between three intervals. In interval #1 (94.56-104.70 m; 93.97-94.26 Ma) there is ~8 kyr between samples based on an astrochronologic time scale for the core (Jones et al. 2019); in interval #2 (104.83-119.00 m; 94.26-94.69 Ma) there is ~5 kyr between samples; and in interval #3 (119.45-122.34 m; 94.69-94.78 Ma) there is ~2 kyr between samples. For assemblage studies, slides were made from more dilute solutions so that counts could be conducted. Nannofossil specimens were observed under a Zeiss Axioskop 2 Plus light microscope at a magnification of 1000x. Specimens one-half the size of a coccolith or larger were considered as one specimen and a total of over 31,000 specimens were counted. However, identification at the species level was not always possible due to taxonomic difficulties along with non-optimal preservation in certain intervals. Counts of 100, 200 and 300 specimens were made in different regions of the same smear slide for one sample and show within 10% difference in the dominant taxa (text-fig. 3). They confirm that a 200-specimen count provides a representative sample of the assemblage. We thus adopted a 200 specimen count instead of a 300 specimen count so that more samples could be investigated. All data are archived on the Pangaea database (https://www.pangaea.de/).

Although 63 species were identified, only 11 species or groups of species within a genus were chosen for detailed paleoecological analysis (Tables 2-4). Species/genus groups were removed from analysis if the taxa amounted to less than 1% of the total sample count throughout the core.

Total Carbon, Total Inorganic Carbon and Total Organic Carbon Analysis

Geochemical analyses were run on the same samples used for nannofossil assemblage studies. One hundred fifty-five samples were powdered using a tungsten ball mill. The ball mill was cleaned with pure sand between samples to prevent contamination. Total carbon, total inorganic carbon, and total organic carbon were analyzed with a UIC coulometer. Weight percent total carbon (TC) values were obtained by combustion at 950°C in a stream of ultra-high purity oxygen using the UIC CM5200 Autosampler/Furnace. Weight percent total inorganic carbon (TIC) values were obtained by acidification with phosphoric acid using the UIC CM5240 TIC Autoanalyzer. The CO_2 liberated by each process was titrated in a coulometer cell to deter-

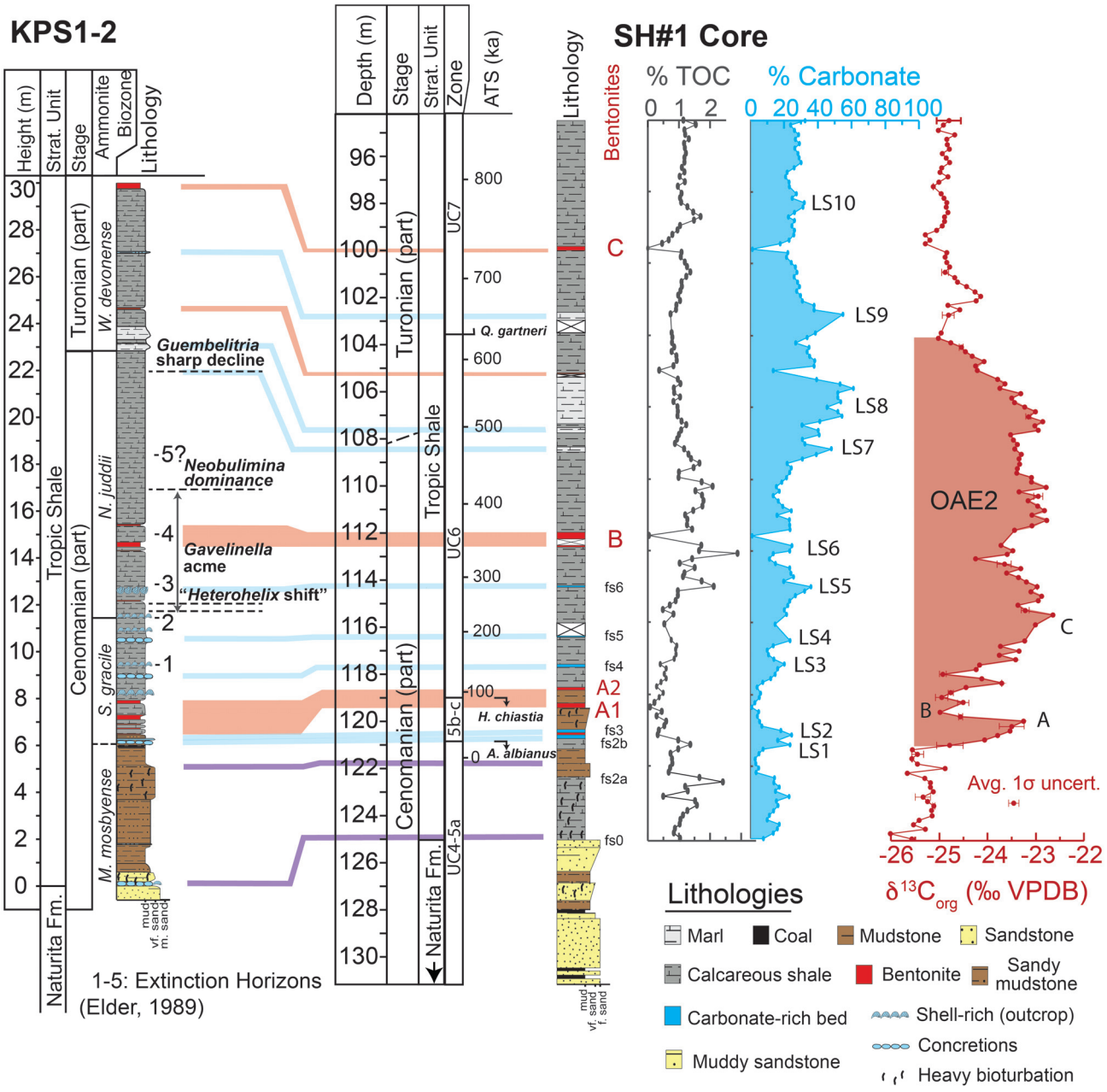

TEXT-FIGURE 2
Stratigraphic column for SH#1 near Big Water, Utah with geochemical data. The Tropic Shale is mainly composed of calcareous shale and mudstone. The depositional environment of the Tropic Shale is a prodeltaic environment within ~150 km of the western margin of the WIS (Leithold 1993). Key foraminiferal events described in the KPS1 and KPS2 outcrops (Parker et al., in review) are correlated to the SH#1 core (after Jones et al. 2019). %TOC and % calcium carbonate were collected at Pennsylvania State University. Stratigraphic column and $\delta^{13}C_{org}$ from Jones et al. (2019). Correlative limestone beds LS1 to LS10 from (Elder 1985) are indicated in $\%CaCO_3$ and blue horizontal lines; bentonites shown in red and pink horizontal lines; purple lines are flooding surfaces; C-isotope stages after (Pratt 1985), nannofossil zones after (Burnett et al. 1998).

mine TC and TIC (Engleman et al. 1985). Weight percent total organic carbon (TOC) values were obtained by calculating the difference between TC and TIC. Weight percent $CaCO_3$ values were calculated from TIC based on stoichiometry of $CaCO_3$. Carbonate standards, in house standards (Devonian Black Shale) and blanks were included in every run to calculate the precision of the coulometric analysis. Data are archived on the Pangaea data publisher (https://www.pangaea.de/).

Trace metal analyses

Fifty-four of the powdered samples were analyzed for trace metal content. Powdered bulk rock sample (0.1 g) was mixed with 0.4 g of lithium methaborate flux. Samples were put into graphite crucibles and put into a muffle furnace at 900°C for 20 minutes so the mixture formed a glass. Once the samples were removed from the oven, they were left to solidify for 30 min-

TABLE 2
Relative abundance values were used to calculate Pearson's correlation coefficients for each of the 11 taxa relative to one another and to the $\delta^{13}C_{org}$, TOC, and $CaCO_3$ values.

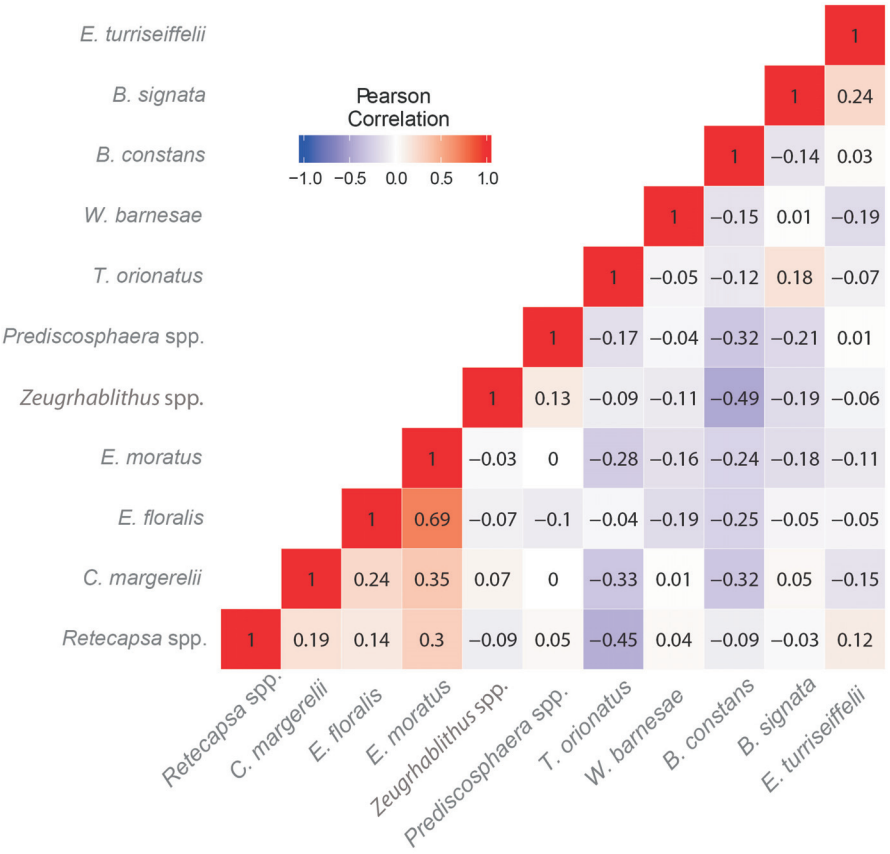

utes. The lithium metaborate beads were then embedded in epoxy in 2.5 cm diameter round discs, and polished to expose a flat surface of glass for analysis via Laser Ablation Inductively Coupled Plasma Mass Spectrometry (LA-ICP-MS). Samples were analysed using a NWR 193 Excimer Laser Ablation System coupled to a Thermo Fisher Scientific X-Series II ICP-MS at the Laboratory for Isotopes and Metals in the Environment (LIME) at The Pennsylvania State University. Samples were ablated with a 150 µm spot at 20 Hz and a fluence of 10J/cm^2 for 30 seconds. Calibrations were achieved using NIST 610, which bracketed every three ablations throughout the run. Samples were ablated twice and the average value was reported. Cody Shale (SCO-1) and Centreville Diabase (W-2) were processed alongside the samples and used as check standards. LA-ICP-MS data were processed using the LasyBoy Version 3.01 in Microsoft Excel. Trace elements were reported normalised to Zr to remove any artifacts due to changing input from terrestrial sources. Data are archived on the Pangaea database (https://www.pangaea.de/).

Statistical Analysis

The structure of calcareous nannofossil assemblages was investigated using Cluster Analysis and Detrended Correspondence Analysis (DCA). These analyses were performed with the program R (www.r-project.org) using the "cluster" (Maechler et al. 2013), "sparcl" (Witten and Tibshirani 2010), and "vegan" (Oksanen et al. 2019) packages. Data were investigated two ways for each type of analysis: using the Q and R-mode in Cluster Analysis and the sites (samples) and species scores in DCA.

The transformation and distance measure chosen for cluster analysis in Q-mode (samples) were the Wisconsin Transformation and the Bray-Curtis Distance. Transformations improve the normal linearity and make variables (i.e. taxa) comparable; distance measures constrain the distance between samples in multivariate space (McCune et al. 2002). The Wisconsin transformation was chosen because it normalizes both rows and columns by the maximum value. The coefficient of variation for rows was 5.78 (low effect) and 87.96 (high effect) for columns. The Bray-Curtis Distance was chosen because it is ideal for analyzing ecological datasets. Additionally, the Bray-Curtis Distance Measure and Ward's method create compact and identifiable groups and produce a high agglomerative coefficient. The agglomerative coefficient expresses the strength of clusters. The clustering method Group Average was also tested, but agglomerative coefficient values were higher with the Wisconsin Transformation, Bray-Curtis Distance and Ward's Method (Fortiz 2017). External variables from the sample attributes matrix were overlain on the sample cluster to find trends in the data (Fortiz 2017). For cluster analysis in R-mode (species), the transformation and distance measure used were Column Maxima and Bray-Curtis Distance. The Column Maxima transformation relativizes values in columns by the highest value. The combination of using Column Maxima Relativization, Bray-Curtis Distance and Ward's Method resulted in the highest agglomerative coefficient value.

The Wisconsin transformation was chosen for DCA because it normalizes both rows and columns by the maximum value.

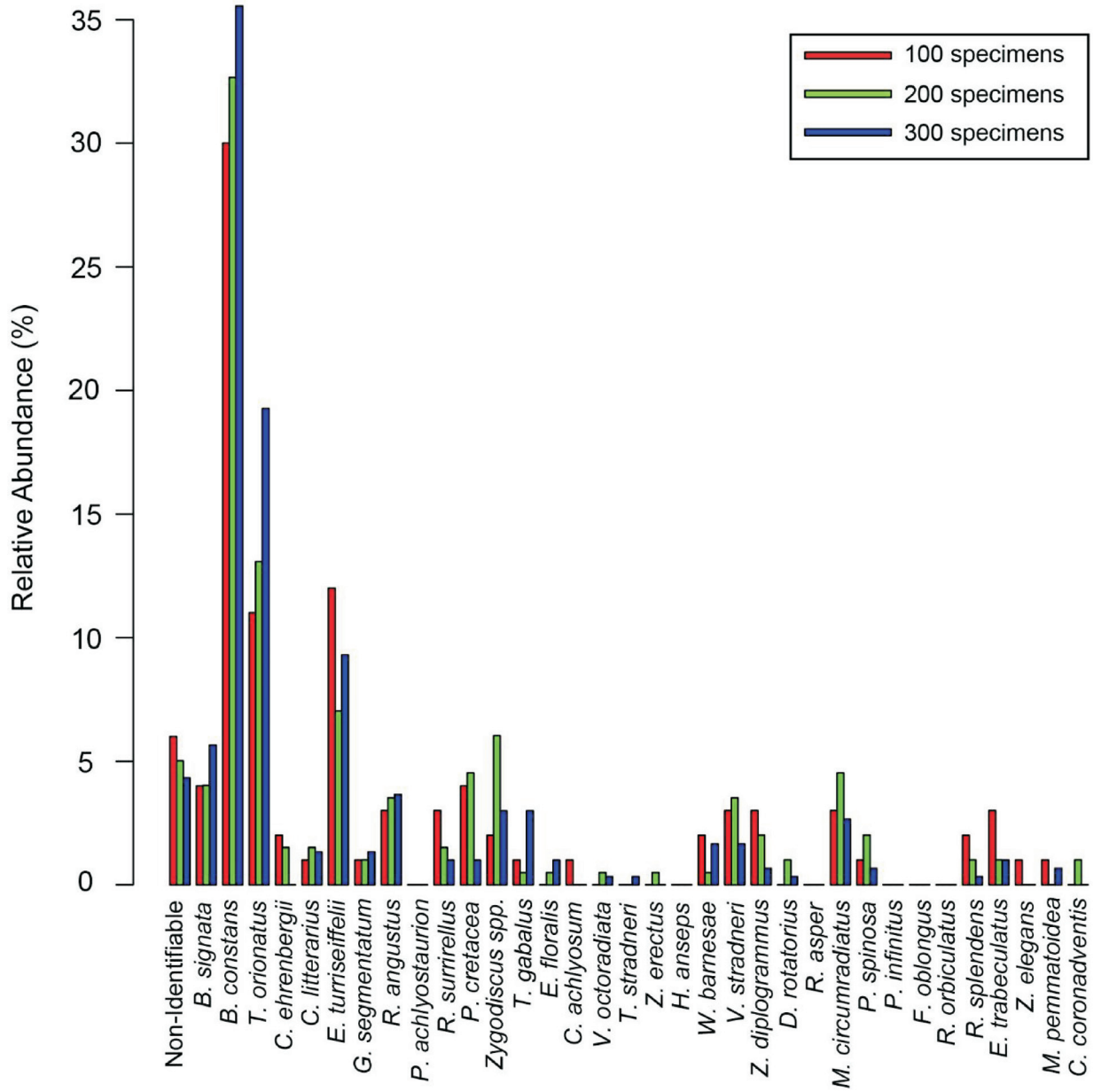

TEXT-FIGURE 3
Relative abundance data for counts of 100, 200 and 300 specimens in different regions of the slide from sample SH#1-66-120.25 m. This comparison indicates that 200 specimens provide a representative sample of the assemblage. Difference between counts are less than 10% of the relative abundance of the sample for each taxa.

DCA uses a Chi-square Distance metric so that the distance between sites and species scores is proportional to their chi-square value. This type of distance metric gives a lot of weight to rare species which was ideal for the Smoky Hollow assemblages. Eigenvalues can be transformed to percent variance by calculating the total of the first four DCA axes and dividing each individual eigenvalue by that total. The percent variance explained for DCA using the Wisconsin Transformation and Chi-square Distance metric for the first four axes are: 43.21%, 22.60%, 19.27%, and 14.92%. External variables from the sample attributes matrix were overlain on site scores to find trends in the data (Fortiz 2017).

Relative abundance values were used to calculate Pearson's correlation coefficients for each of the 11 taxa relative to one another and to the $\delta^{13}C_{org}$, TOC, and $CaCO_3$ values (Tables 2, 3).

RESULTS

Calcareous Nannofossil Biostratigraphy

The CTB interval markers in the SH#1 core were generally very rare compared to sections from the central part of the WIS, including the Carthage outcrop section in New Mexico (Bryant 2021), and the Portland and Rebecca Bounds cores in Colorado and Kansas, respectively (Bralower and Bergen 1998). Markers

TABLE 3
Correlation of nannoplankton taxa with TOC (%) and $CaCO_3$ (%).

	TOC (%)	CaCO3 (%)
B. constans	-0.12	0.1
B. signata	**0.17**	**0.42**
E. turriseiffellii	0.06	**0.14**
T. orionatus	0	-0.12
Zeugrhabdotus spp.	0.14	-0.12
W. barnesiae	0.06	**0.16**
Retecapsa spp.	**0.18**	0.08
Prediscosphaera spp.	0.11	**-0.17**
E. floralis	**0.25**	**-0.19**
E. moratus	0.1	-0.3
C. margerelii	**0.17**	0.14

Bold are correlations that are significant at the 95% confidence level

are equally rare as in other sections along the western margin of the seaway, including the Escalante Core (Bralower and Bergen 1998). Markers observed in the central seaway including *Lithraphidites acutum, Corollithion kennedyi* and *Eiffellithus eximius* are not observed in SH#1 samples likely because of the more coastal environment. The most useful markers*, Axopodorhabdus albianus* and *Helenea chiastia,* are very rare in SH#1 compared to central WIS sections, having sporadic occurrences. We identify the last occurrences of *Axopodorhabdus albianus* (between 118.8 and 118.6 meters) and *Helenea chiastia* (between 117.49 and 117.09 meters) at levels reported by Jones et al. (2019) (Table 1; text-fig. 2). The combined subzones UC5b and UC5c of Burnett et al. (1998) lie between these datums. The lower part of the section lies in Subzone UC5a and Zone UC4. The upper part of the section largely corresponds to Zone UC6 of Burnett et al. (1998) (Figure 2). We identify the first occurrence of *Quadrum gartneri* between 104.5 and 103.6 meters, although this species occurs very sporadically in the early part of its range and we tentatively place the base of Zone UC7 at this level.

Calcareous Nannofossil Assemblages

The calcareous nannofossil assemblage composition shows distinct changes during the Carbon Isotope Excursion (CIE) that defines the chemostratigraphic extent of OAE2 between 121.15 m and 103.69 m in the SH#1 Core (Jones et al. 2019) (text-figs. 4 and 5). The relative abundance of *Biscutum constans* is high but variable before and after the excursion and generally low between 119.95 m to 106.29 m which coincides with all but the top of the CIE (text-fig. 4a, b). *Zeugrhabdotus* spp. has relatively high and variable abundance without strong trends except a minor increase in abundance between 113.5 m and 106.9 m is recorded, as is a decrease in the uppermost lower Turonian above the CIE from 99.29 m to 95.69 m (text-fig. 4c). *Tranolithus orionatus* shows a slight increase in relative abundance during the CIE from 121.11 m to 106.50 m with a sharp increase in one sample at 110.50 m and significant variation after the excursion (text-fig. 4d). *Watznaueria barnesiae* shows cyclic changes in relative abundances throughout the study interval (text-fig. 4e) with a decrease between the base of the section and 120.0 m, followed by an increase to 115.6 m, then a decrease to 109.3 m, followed by an increase to 106.7 m, then relatively level abundance to the top of the section.

The relative abundance of *Broinsonia signata* shows significant variation but increases during the CIE from 118.00 m to 112.6 m, from 110.30 m to 102.28 m, and above the excursion in the uppermost lower Turonian from 100.50 m to 94.90 m (text-fig. 5b). *Eiffellithus turriseiffelii* fluctuates throughout the study interval ranging from 0% at 122.26 m to 11% at 119.66 m (text-fig. 5c). The relative abundance of *Prediscosphaera* spp. shows short-term increases before and during the CIE from 122.34 m to 103.69 m with a decrease at the top of the excursion and significant variation in lower Turonian sediments (text-fig. 5d). *Retecapsa* spp. fluctuates throughout the study interval with an overall, slight increase in abundance from 119.55 m to 101.90 m and an increase into the uppermost lower Turonian (text-fig. 5e). The relative abundances of *Eprolithus floralis* and *E. moratus* show variations throughout the section with a sharp increase during the CIE between 113.50 m and 103.52 m comprising a major peak of abundance between 113.3 and112.9 m and a minor peak between 110.9 and 108.1m (text-fig. 5f, g); these peaks are informally termed "blooms" here. Finally, *Cyclagelosphaera margerelii* shows a sharp decrease in abundance just below the base of the CIE (text-fig. 5h). The remainder of the section shows strong cyclic changes in this species with increases between 120 and 113.9 m, 109.7 m and 107.3 m, and 103.7 m and 100.9 m, and decreases between 113.9 m and 109.7 m and 107.3 m and 103.7 m. The intervals with increased *C. margerelii* generally correlate with three intervals of higher $CaCO_3$% (text-fig. 2).

Geochemistry

Percent TOC and %$CaCO_3$ changes observed are similar to those described by Jones et al. (2019) although samples are offset by a couple of centimeters in some intervals (Fortiz 2017). TOC values range from 0.20% to 2.20% (text-fig. 2). Mean and standard deviation for TOC for the whole section are 0.98% and 0.41%, respectively. There is a short-term and minor increase in values at the onset of the CIE at 121.05 m with a sharp decrease thereafter, from 2.07% to 0.23%; low values continue throughout the lower part of the CIE from 120.85 m to 115.19 m. %TOC increases during the middle to upper part of the CIE from 115.19 m to 105.50 m with a mean of 1.27%. At the top of the CIE, %TOC decreases to a mean of 1.10% but is still higher than at the onset of the excursion.

%$CaCO_3$ ranges from 2.17% to 57.48% (text-fig. 2) with mean and standard deviation of 21.21% and 12.91%, respectively. There is an increase at the onset of the CIE at 121.05 m with a sharp decrease thereafter. Percent $CaCO_3$ is low from 120.45 m to 118.40 m with a mean of 6.45%, and variable during the early to middle stages of the CIE from 118.40 m to 110.10 m with a mean of 19.62%. Near the top of the CIE, %$CaCO_3$ increases to a mean of 34.81% and values are high from 109.90 m to 100.09 m into the mid-lower Turonian, and constant thereafter with an average of 26.36%, higher than pre-CIE values.

Trace metals were separated out into non-volatile (Sc, Co, Cr; text-fig. 6b) and volatile elements (Cu, Pb; text-fig. 6c) with oceanic residence times of 10–10,000 years following the classification of Rubin (1997). Non-volatile elements (text-fig. 6b) increase above the first step (Step A of Pratt 1985) increase in $\delta^{13}C$ at 119.5 m, reaching a peak at 116.5 m before decreasing to a constant level from 117 to 98.5 m, which is 1.5–2 times higher than before the onset of OAE2. The volatile elements (text-fig. 6c) are noisier throughout the section. There are two main peaks in Cu/Zr, at 116.5 m and 111.5 m, and one main peak in Pb/Zr at

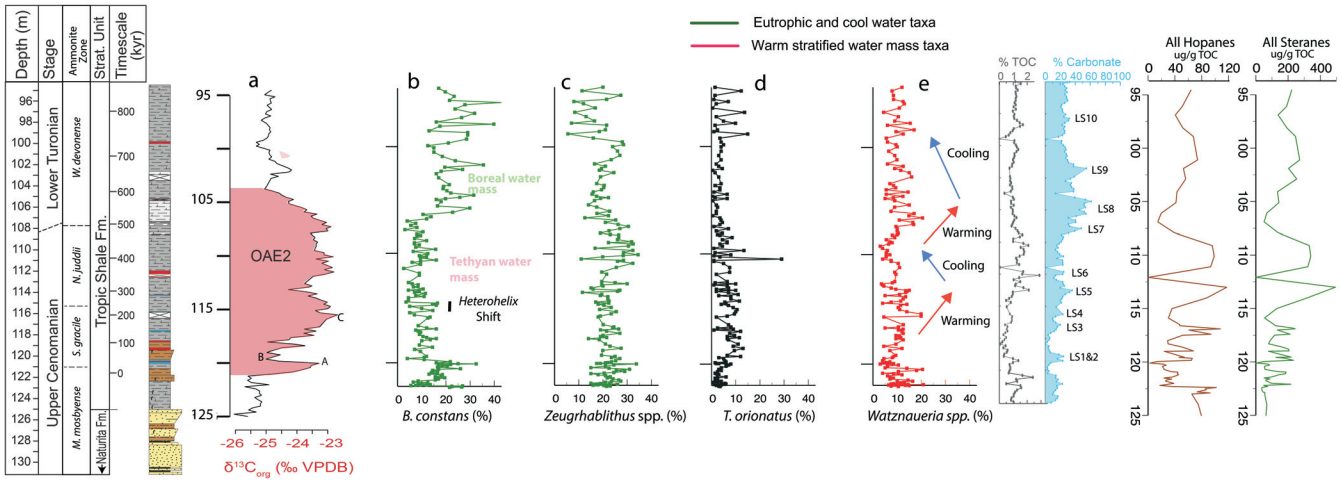

TEXT-FIGURE 4
Relative abundance patterns of higher abundance calcareous nannofossils in the Cenomanian/Turonian Boundary interval from the SH#1 core. Included is the relative timescale, stratigraphic log (exed out intervals represent core gaps) and δ $^{13}C_{org}$ values (Jones et al. 2019). Relative abundance lines are coded by the taxon's paleoecological affinity: green- eutrophic and cool water taxa and red- oligotrophic and warm water taxa; black refers to taxa whose affinities differ among authors (Table 4) and as a result of this investigation. Extent of OAE2 is based on the CIE shown in red in Column A. Biomarker data from Boudinot et al. (2020). Interpretation of water masses and warming and cooling phases based on the abundance of *W. barnesiae* along with correlation to %$CaCO_3$.

111.5 m. Levels of volatile trace metals from 117 to 98.5 m are 1.4–1.8 times higher than before the onset of OAE2. Increases in both the volatile and non-volatile volcanogenic trace metals records occur stratigraphically higher than the initial osmium isotope (Os_i) excursion and ^{192}Os spikes (Jones et al. 2021) in SH#1, which have been used as characteristic markers for the initiation of volcanic activity bracketing the onset of OAE2 (Turgeon and Creaser 2008) (text-fig. 6).

Statistical Analysis

Cluster Analysis- The cluster analysis of taxa yielded two primary groupings throughout the section: one containing more abundant species and/or genera and the other containing rarer species and/or genera (text-fig. 7). Each of these clusters can be further subdivided into three groupings. The low abundance taxa clusters include: (1) *B. signata* and *E. turriseiffelii*; (2) *Retecapsa* spp. and *C. margerelii*; and (3) the "bloom" taxa *E. floralis* and *E. moratus*. The high abundance clusters consist of: (1) *B. constans* and *Zeugrhabdotus* spp. and (2) *W. barnesiae* and *Prediscosphaera* spp.; while (3) *T. orionatus* is in a separate cluster from other taxa.

Detrended Correspondence Analysis- DCA 1 accounts for 43.21% of the variance in the original matrix and DCA2 accounts for 22.60%. Axis DCA1 and DCA2 separate *B. constans* which has negative DCA1 and DCA2 scores from other taxa (text-fig. 8). Additionally, we find a group of species including *C. margerelii*, *E. floralis*, and *E. moratus* having high DCA1 and DCA2 scores.

DISCUSSION

Non-ecological Factors: Preservation and the closed-sum effect

Nannofossil preservation and relative abundance are altered during diagenesis (Thierstein and Roth 1991). Preservation throughout the SH#1 section is generally moderate to excellent with no clear visual variation in alteration upsection. Changes in $CaCO_3$%, abundance of dissolution-resistant taxa such as *Watznaueria barnesiae* and species of *Eprolithus* (Thierstein 1980; Roth and Krumbach 1986; Williams and Bralower 1995) can also be used to determine changes in preservation that are not observed microscopically and that might impact species variation. The abundance of *W. barnesiae* is commonly used to interpret preservational changes in Cretaceous samples (Hill 1975; Roth and Bowdler 1981). Previous studies have interpreted high abundances of *W. barnesiae* (>40% (Thierstein 1981; Roth and Krumbach 1986); >70%, (Williams and Bralower 1995) as an indicator of poorly preserved assemblages. Low relative abundance of *W. barnesiae* (mean = 10%) at SH#1 confirms the well-preserved nature of the nannofossil assemblage. Additionally, the mean abundance of *Eprolithus* spp., another solution-resistant taxon, is 3.32% and samples with abundant *Eprolithus* spp. do not coincide with those with abundant *W. barnesiae* (text-figs. 4 and 5). Based on the lower relative abundance of *W. barnesiae,* nannofossil preservation in SH#1 appears to be better than in the Portland core (mean= 43.91%) and the Bounds core (mean= 26.65%) (Burns and Bralower 1998) (Figure 1).

The relationship of %$CaCO_3$ with calcareous nannofossil preservation is not clearly understood. Previous studies of deep-sea sections have indicated that samples with $CaCO_3$ greater than 60% generally have overgrown nannofossils while samples with $CaCO_3$ less than 40% have etched nannofossils (Thierstein and Roth 1991). In nearshore settings $CaCO_3$ is also controlled by siliciclastic dilution so relationships with preservation are more complicated. In SH#1 $CaCO_3$ is mostly below 40%, especially in samples around the four bentonite layers, and never exceeds 60% (text-fig. 2), suggesting more etching than overgrowth. *W. barnesiae* shows a weak positive correlation (95% confidence level) with %$CaCO_3$ (Table 3). On the other

TABLE 4
Published paleoecological interpretations of nannoplankton taxa.

Species/Genus	Trophic Level Affinity	Temperature/Other affinities	References
B. constans	Eutrophic	Cool waters	Roth and Bowdler, 1981; Thierstein, 1981; Roth and Krumbach, 1986; Watkins, 1986; Erba et al., 1992; Linnert and Mutterlose, 2015
W. barnesiae	Oligotrophic	Warm waters	Roth and Krumbach, 1986; Linnert and Mutterlose, 2015
T. orionatus	Mesotrophic/Eutrophic	Cool waters	Roth, 1981; Linnert and Mutterlose, 2015
Broinsonia spp.	Oligotrophic, stratified water1	Nearshore2	1 Hardas and Mutterlose, 2007; Linnert and Mutterlose, 2013; 2 Roth, 1981; Roth and Bowdler, 1981; Roth and Krumbach, 1986
E. turriseiffelii	Oligotrophic		Watkins, 1989; Eleson and Bralower, 2005
Eprolithus spp.		Cool waters1; stratified waters2	1 Roth and Krumbach, 1986; Lamolda et al., 1994; 2 Hardas et al. 2012
Retecapsa spp.	Oligotrophic	Warm waters	Thierstein, 1981; Eleson and Bralower, 2005
Prediscosphaera spp.	Mesotrophic/Eutrophic1; Oligotrophic2	Cool waters1	1 Thierstein 1981; Eleson and Bralower, 2005; 2 Watkins et al., 1989, Eshet et al., 1992, and Eshet and Almogi-Labin, 1996, and Hardas et al., 2012
Zeughrabdotus spp.	Eutrophic		Roth, 1989. Watkins, 1989; Erba et al., 1992

hand, the two *Eprolithus* species, *E. floralis* and *E. moratus*, have a weak negative correlation (95% confidence level) and a moderate negative correlation (99% confidence level) with $\%CaCO_3$, respectively (Table 3). We therefore conclude that assemblage variations are not a result of changes in carbonate preservation but acknowledge that siliciclastic dilution weakens this conclusion.

Calcareous nannofossil assemblage interpretation can be complicated by the "closed-sum effect", whereby high abundances or an increase of one species resulting from primary or diagenetic factors may directly influence the abundances of other taxa. For example, low abundance of the dissolution-susceptible *Biscutum constans* could result from an increase in the dissolution-resistant *W. barnesiae* due to preferential preservation of the less susceptible species. On the other hand, the low percentage of the taxon *B. constans* may be caused by paleoecologic/paleoceanographic changes independent of an increase in percentage of another taxon. Overall, the "closed-sum" problem is more prevalent in sections other than SH#1 where the preservation is poor throughout and the abundance of dissolution-resistant taxa, like *W. barnesiae*, is high.

Interpretation of calcareous nannofossil paleoecology

Over the past 30 years, studies have constrained the affinities of certain nannofossil species to variations in temperature and productivity (Roth 1981; Thierstein 1981; Roth and Bowdler 1981; Roth and Krumbach 1986; Silvá et al. 1989; Roth 1989; Watkins 1989) The two most commonly accepted Cretaceous species affinities are that of *Biscutum constans* with higher surface-water productivity (eutrophic conditions) and generally cooler waters and *Watznaueria barnesiae* with warmer waters and low surface-water productivity (oligotrophic conditions) (Thierstein 1981; Roth and Krumbach 1986; Silvá et al. 1989; Erba et al. 1992; Lees 2002; Eleson and Bralower 2005; Linnert and Mutterlose 2015). These affinities are based on the geographic distributions with the abundance of *B. constans* being highest at sites in upwelling environments along continental margins and higher-latitude settings, and *W. barnesiae* being most common in nutrient-poor central gyres and lower-latitude settings. However, both temperature and nutrient levels are distributed along continua, for example the trophic resource continuum of (Hallock 1987). Thus, even though temperature and productivity have been traditionally coupled in interpretations of paleoecology, it is entirely possible that the abundance of taxa was a response to one variable, for example, warm temperature over another, for instance low nutrient levels.

Species belonging to *Zeugrhabdotus* were also generally found to occur in upwelling environments and correlate modestly with the abundance of *B. constans*, thus this taxon is also accepted as an indicator of cooler water conditions and high productivity (Watkins 1989). However, other species generally have less clear geographic distributions and paleoecologic affinities, although associations with different conditions have been made (see summary in Table 4); we apply these associations with a degree of skepticism and further probe their paleoecology. Of particular interest is the abundance of the solution-resistant "bloom taxa" *Eprolithus* spp. which has been related to dissolution (Hill 1975; Roth and Krumbach 1986; Bralower 1988; Williams and Bralower 1995) but has also been proposed to be adapted to cool waters (Roth and Krumbach 1986; Lamolda et al. 1994) as well as oligotrophic, stratified water masses (Hardas et al. 2012). Also, *Broinsonia signata* has been interpreted to be a species that is adapted to nearshore environments (Roth and Krumbach 1986) as well as oligotrophic, stratified waters (Hardas and Mutterlose 2007; Linnert and Mutterlose 2015), and shows abundance peaks in the northern part of the WIS (Bralower 1988). Finally, *Cyclagelosphaera margerelii* is thought to have been adapted to eutrophic but seasonally stratified water columns (Lees et al. 2004). Here we investigate the paleoecology of nannoplankton in the SH#1 core first using multivariate statistical analysis, and then using comparison with foraminiferal assemblages and organic biomarkers.

Statistical analysis of nannofossil assemblage data: The cluster dendrogram shows a split between the well-established eutrophic-mesotrophic and cool water taxa and oligotrophic and warm water taxa (text-fig. 7) with *B. constans* and *Zeugrhabdotus* spp. aligning and in a different cluster from *W. barnesiae*. The paleoecology of species with less well-known affinities can be interpreted from those of the nearest neighboring taxa. For example, the ecology of *E. turriseiffelii* can be ascertained from its neighbor, *B. signata*, a proposed nearshore or oligotrophic/stratified water mass indicator (Hardas and Mutterlose 2007; Roth and Bowdler 1981). This comparison yields similarities to previous interpretations (Table 4) along with some differences. For example, *Prediscosphaera* spp., which has been interpreted as adapted to oligotrophic as well as eutrophic and possibly cool waters (Table 4), clusters with *W. barnesiae,* which was adapted to warm, oligotrophic waters. Moreover, affinities of the "bloom taxa", *E. floralis* and *E. moratus*, cannot be determined from cluster analysis because these taxa are in a separate cluster from those with established paleoecological affinities.

To further address the paleoecology of species, we interpret their DCA1 and DCA2 scores (text-fig. 8). Taxa grouping at the center of the DCA plot are those present with relatively even abundances in most samples including *W. barnesiae* and *Zeugrhabdotus* spp, and their ecology cannot be interpreted

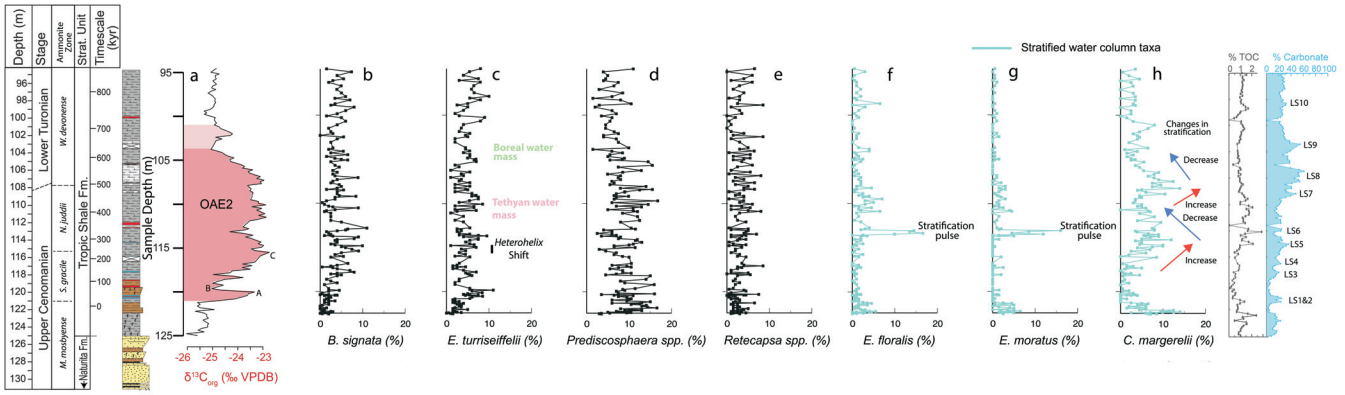

TEXT-FIGURE 5
Relative abundance patterns of lower abundance calcareous nannofossils in the Cenomanian/Turonian Boundary interval from the SH#1 core. Included is the relative timescale, stratigraphic log (exed out intervals represent core gaps) and $\delta^{13}c_{org}$ values (Jones et al. 2019). Relative abundance lines are coded by the taxon's likely paleoecological affinity: light blue- warm and stratified water mass taxa, black refers to taxa whose affinities differ among authors (Table 4) and as a result of this investigation. Extent of OAE2 is based on the CIE shown in red in Column A. Stratification pulse based on blooms of *Eprolithus* spp. and warming and changes in stratification based on fluctuations in the abundance of *C. margerelii* are also shown along with correlation to $\%CaCO_3$.

from the DCA data alone. Negative DCA1 values correspond to taxa thought to be adapted to eutrophic and cool waters (Table 4) including *B. constans* and *T. orionatus*, and nearshore environments including *B. signata*. More positive DCA1 values include taxa thought to be adapted to oligotrophic and warm water environments such as *Retecapsa* spp. and *Prediscosphaera* spp. in some interpretations (Table 4), but also taxa that are thought to be adapted to cooler and/or more eutrophic waters including *Prediscosphaera* spp. in other interpretations (Table 4). The "bloom taxa" *E. floralis* and *E. moratus,* and *C. margerelii* have the highest DCA1 values suggesting adaptation to warmer and more oligotrophic waters though possibly both taxa thrived at least seasonally in a stratified water mass rather than any other variable (Lees et al. 2004; Hardas et al. 2012). Biomarker data from the SH#1 core suggest that productivity may actually have been high during this interval (Boudinot et al. 2020), indicating that oligotrophy alone likely does not explain the bloom taxa values. DCA2 does not appear to show a clear relationship with an ecological or preservational variable.

The statistical results generally confirm previous interpretations of nannofossil ecology especially for taxa with well-established affinities (*B. constans*, *Zeugrhabdotus* spp. and *W. barnesiae*) and to a degree those with less well-established affinities (i.e., *B. signata, T. orionatus*, *Eiffellithus turriseiffelii and Prediscosphaera* spp.). However, interpretation of these and other taxa benefits from comparison with foraminiferal assemblages and biomarker data.

Comparison with foraminiferal assemblage and biomarker data: Extensive investigations of planktic and benthic foraminifera in the WIS provides compelling information on water mass properties and how they changed through time (Eicher and Worstell 1970; Leckie 1985; Eicher and Diner 1985; Leckie et al. 1991; Leckie et al. 1998; Lowery et al. 2014; Elderbak and Leckie 2016). The western WIS margin had a distinct circulation pattern with pulses of southern Tethyan waters alternating with pulses of cool Boreal waters (e.g., Leckie et al. 1998), the timing of these events is generally well constrained.

The carbonate-rich beds in the middle of the section (correlative to LS5-8) contain planktic foraminiferal assemblages thought to reflect the incursion of a warmer, more normal marine Tethyan water mass along the western WIS margin, and the upper part of the section (above the equivalent to bed LS9) contains assemblages becoming more indicative of Boreal water masses as defined by increasing, and then decreasing relative abundances of *Muricohedbergella* spp. (Leckie et al. 1998). A prominent, basinwide shift in planktic foraminiferal assemblages occurs near the equivalent of limestone bed LS5 (114.9 m), with a sharp increase in the abundance of the biserial planktic foraminiferal genus *Planoheterohelix* spp. (Leckie 1985; Leckie et al. 1991, 1998; Lowery et al. 2014; Elderbak and Leckie 2016; Bryant 2021) across the WIS. This "*Heterohelix* shift" is temporally related to changes in benthic foraminiferal assemblages ("*Gavelinella* acme") and has been attributed to increased runoff and high productivity, development of photic zone euxinia, and cabbeling (e.g., Leckie et al. 1998; Elderbak and Leckie 2016; Boudinot et al. 2020; Bryant et al. 2021). The "*Heterohelix* shift" occurs just below the intervals of elevated abundances of *Eprolithus* spp. at 113 m and in the interval from 111-108 m (text-fig. 5f,g) and coincides with the onset of elevated abundance of *C. margerelii* (text-fig. 5h). Planktic foraminiferal assemblages corresponding to these peaks include generally warmer-water assemblages (e.g., Elderbak and Leckie 2016; Bryant et al. 2021).

A brief interval near the base of the SH#1 section between ~120 and 116 m (isotope stages B and C of Pratt 1985) is thought to correlate with the Plenus cooling event in northern Europe based on the carbon isotope profile (Boudinot and Sepúlveda 2020; Boudinot et al. 2020). Interestingly this interval lies above the initial increase in the abundance of the *B. constans* in isotope stage A of Pratt (1985), which suggests that the occurrence of cooler Boreal waters along the WIS margin predated the Plenus step. While in European and Atlantic sites, the Plenus event is associated with the incursion of cool waters and thus its association with cooling (see review in (Jenkyns 2018), in the WIS, the step involves an invasion of warm Tethyan waters in the central (Elderbak and Leckie 2016; Bryant et al.

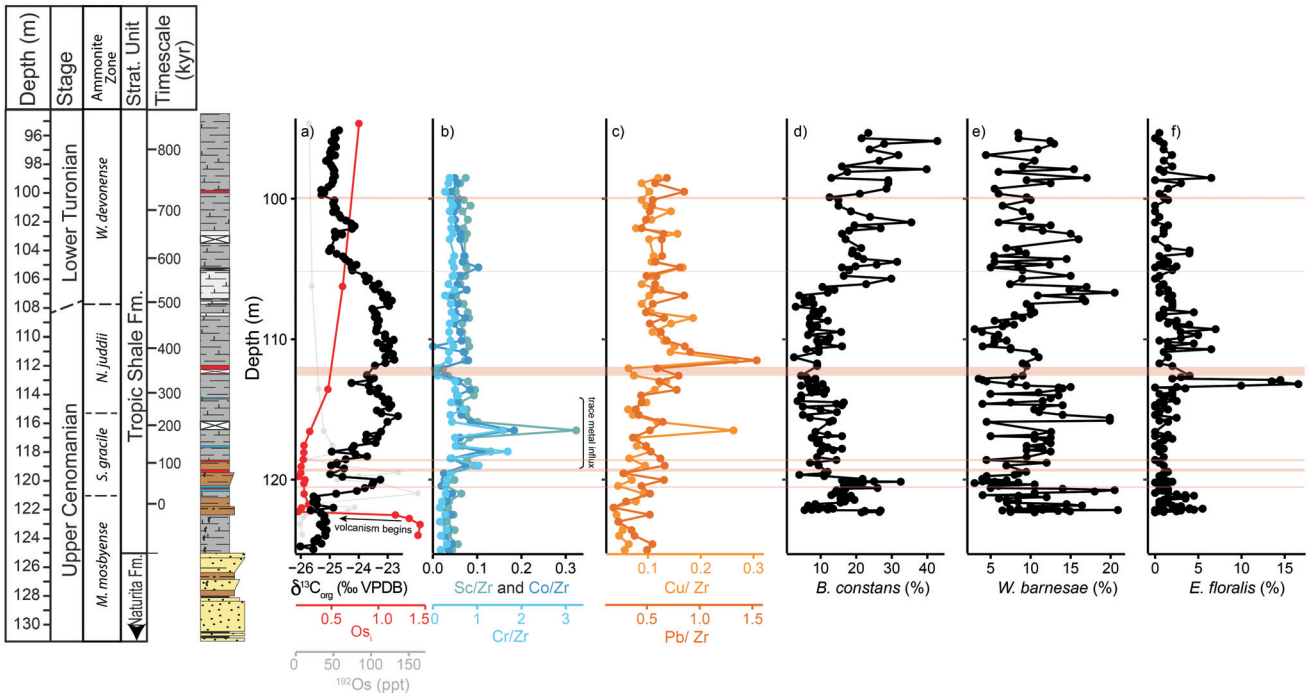

TEXT-FIGURE 6
Changes in trace metal concentrations and nannofossil abundances through OAE2 on the western margin of the Cretaceous WIS: a) bulk organic carbon isotopes ($\delta^{13}C_{org}$), initial osmium isotopes (Os_i), and ^{192}Os contents from the SH#1 core: (Jones et al. 2019; Jones et al. 2021) are plotted to show the character of the event in this location. Trace metals are normalized relative to Zr and are separated into b) non-volatile trace metals, and c) volatile trace metals following Rubin (1997). Each colored line represented a different element. Calcareous nannofossil abundances are represented by d) *B. constans*, a eutrophic species, e) *W. barnesiae*, an oligotrophic and warm water species, and f) *E. floralis*, a bloom species. There is no correlation between trace metal concentrations and calcareous nannofossil abundances. Pink lines refer to bentonites (see text-fig. 2).

2021) and western part of the seaway (this study). This is consistent with other studies that show that the Plenus cooling varied significantly by location and that in some locations the event involved a less intense hydrologic cycle rather than cooling (O'Connor et al. 2020; Lowery et al. 2021).

Biomarkers show a prominent decrease in the abundance of freshwater algae and reorganization of algal communities coincident with the late Cenomanian transgression (Boudinot et al. 2020). These changes also coincide with the appearance of nannoplankton in the SH#1 core just below 122 m. The abundance of algal and bacterial biomarkers increases between 115 and 108 m (text-fig. 4) which is indicative of increased productivity along the western margin of the WIS, and this interval also includes compounds that indicate periodic photic zone euxinia and increased water column stratification (Boudinot et al. 2020). This interval corresponds to the blooms of *Eprolithus* spp. and the long-term increase in the abundance of *C. margerelii*. We follow the environmental interpretation of Boudinot et al. (2020) and the paleoecological interpretations of Hardas et al. (2012) and Lees et al. (2004) in interpreting that these taxa were adapted to at least a seasonally stratified water column. Biomarker data also suggest that this interval was characterized by productive surface waters, possibly resulting from an intensified hydrological cycle and increased run-off (Boudinot et al. 2020). This increased productivity agrees with the ecological interpretation of *C. margerelii* of Lees et al. (2004) and further leads us to resolve the ecology of the dominant warm water species in this interval, *W. barnesiae* which has generally been interpreted as adapted to warm and oligotrophic waters (Table 4). We suggest instead that it proliferated in the warm, stratified but productive waters along the western margin of the WIS.

In summary, the environmental framework provided by foraminiferal assemblages and biomarkers allows us to refine the paleoecological affinities of some of the major nannoplankton assemblage markers in the SH#1 core (text-fig. 5). While *B. constans* agrees with the interpretation based on foraminiferal assemblages that cool Boreal waters dominated during the deposition of sediments at the base and top of the section, the dominant taxa in the middle of the section (*W. barnesiae, C. margerelii* and *Eprolithus spp*.) likely proliferated in warm, stratified but productive water masses. Paleoecology of other taxa has been refined somewhat but will require further investigation to be more fully resolved.

Interpretation of trace metal concentrations

Elevated trace metal concentrations in seawater have been suggested to have impacted primary productivity during ocean anoxic events including OAE2, either through fertilization (Leckie et al. 2002; Erba 2004; Erba et al. 2015; Faucher et al. 2017; Zeng et al. 2018; Bottini and Faucher 2020) or trace metal toxicity (Kerr 1998). Volatile trace metals are enriched in magmatically degassed fluids and non-volatile trace metals are concentrated via water-rock exchange reactions at hydrothermal vents (Orth et al. 1993; Rubin 1997; Snow et al. 2005). We assume that the trace metal content reflects concentrations in the

water column at the time of deposition rather than precipitation of diagenetic phases such as pyrite (Brumsack 2006). Both volatile and non-volatile trace metals increase following the first positive carbon isotope excursion (Step A of Pratt (1985)), coincident with the second (and major) positive carbon isotope excursion (Step C) (text-figs. 6b, 6c). At Rock Canyon, a more distal site in the WIS, Orth et al (1993) and Snow et al. (2005) found increased trace metal concentrations were coincident with positive carbon isotope excursions. The SH#1 core is more proximal than the Rock Canyon section (text-fig. 1), and therefore the trace metals may have been consumed by the higher rates of biological activity and sedimentation. The correlation of volatile and non-volatile trace metal concentrations with the main carbon isotope excursion, as at Rock Canyon, suggests that increased trace metal concentrations may have facilitated increased productivity through OAE2 on a global scale as it is thought to have done during early Aptian OAE1a (Erba et al. 2015).

The variability in trace metal concentrations through the section implies that the source of these trace metals was likely pulsed through OAE2, rather than constant over time, although concentration may also be a function of changes in sedimentation rate. This finding is consistent with multiple peaks in ^{192}Os and a prolonged nonradiogenic excursion in initial Os isotopes (Os_i) documented in the SH#1 core, and is a proxy for submarine LIP activity with <30 kyr residence time in the global ocean (Jones et al. 2021). The variability in trace metal concentration data also corroborate the findings of Snow et al. (2005) from Rock Canyon who suggested that the sporadic nature of the emplacement of the Caribbean LIP (Turgeon and Creaser 2008) drove the variability in trace metal concentrations in the WIS. At a finer scale in the SH#1 Core, the volcanogenic trace metal spikes occur several meters above the base of the Os_i excursion (text-fig. 6). This staggered progression between Os_i excursion and trace metal delivery is also noted in Rock Canyon, where (Holmden et al. 2016) attributed the delayed arrival of Cr to the time necessary to weather the freshly emplaced LIP basalts and liberate hydrothermal trace metals. The new record from SH#1 supports this scenario of leached trace metals arriving in the WIS ~80-210 kyr after the beginning of the OAE2 CIE, and ~150-260 kyr after the beginning of the main pulse of activity from the Caribbean LIP.

Despite the coeval increase in trace metal concentrations and the $\delta^{13}C$ excursion at SH#1, there is no correlation between changes in trace metal concentration and the abundances of calcareous nannoplankton. Although we might expect the concentrations to correlate with the abundance of the eutrophic taxon *Biscutum* spp., this is not the case. This suggests that the amounts of trace metals reaching the western margin of the WIS were not high enough to impact the growth of calcareous nannoplankton. Erba (2004) hypothesized that the decline in *B. constans* was a result of metal toxicity, but this is not borne out by the data collected here.

Paleoceanographic significance of changes in calcareous nannofossil assemblages during OAE2

Assemblages in SH#1 indicate significant changes in surface water environments and ocean circulation during OAE2. The most notable change involves the eutrophic and cool water taxon *Biscutum constans* which increases in relative abundance by more than 20% near the onset of the event (text-fig. 4). In addition, as $\delta^{13}C_{org}$ values return to pre-OAE2 values towards the end of the event, there is a ~15% increase in relative abundance of *B. constans*. Interestingly, *C. margerelii* increases concomitant with *B. constans* (text-fig. 5) consistent with its eutrophic assignment (Lees et al. 2004). Although other suspected mesotrophic/eutrophic taxa such as *Zeugrhabdotus* spp., *T. orionatus*, *B. signata*, and *E. turriseiffelii* do not exhibit similarly pronounced trends (text-figs. 4 and 5), we interpret the intervals of increased *B. constans* as successive pulses of Boreal waters along the western margin of the WIS, first near the very onset of OAE2 and then as the event drew to a close. The later phase has previously been interpreted from foraminiferal assemblages (e.g., Leckie et al. 1998) but neither phase has been previously observed in nannofossil assemblages. The Boreal advances are consistent with model simulations (Slingerland et al. 1996; Clark 2018) and foraminiferal assemblage data (e.g., see summary in Elderbak and Leckie 2016) that indicated counter-clockwise surface-ocean circulation.

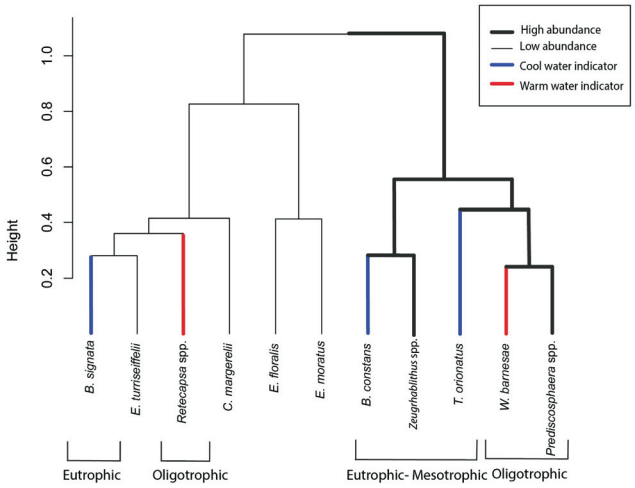

TEXT-FIGURE 7
Cluster analysis of species and genera for the entire dataset. Species and/or genera divide into two main groups: high abundance and low abundance in the section. These main groups can be further subdivided into subgroups by environment. These descriptions are based on the overall paleoecological affinities of the species and/or genera included within the grouping (see Table 4).

In between the Boreal pulses, the SH#1 location was bathed by a warm Tethyan water mass as suggested by the abundance of the warm-water species *W. barnesiae* (text-fig. 4). *W. barnesiae* appears to track $\%CaCO_3$ (text-fig. 4) as does *C. margerelii* to a lesser degree (text-fig. 5). As described, we interpret these taxa as adapted to stratified surface waters at the height of OAE2 in concert with biomarker data (Boudinot at al. 2020). We postulate that this stratification peaked during the blooms of *Eprolithus* spp. which also coincide with peaks of biomarkers for photic zone euxinia (Boudinot et al. 2020). One of the most compelling results of our investigation is the discovery that fluctuations in *W. barnesiae* and *C. margerelii* are quasi-cyclic and correlate moderately well with $\%CaCO_3$, with peaks aligning with the correlative limestone beds (text-figs. 4 and 5). The

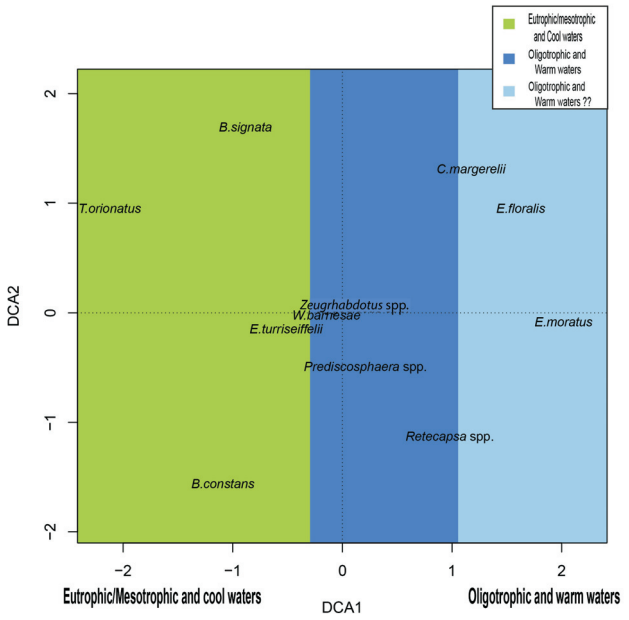

TEXT-FIGURE 8
DCA plot showing species and genera across OAE2 for the SH#1 core. The groupings are labeled by paleoecological affinity (DCA1) of the taxa.

origin of short-term (i.e., bedding couplet) limestone-marl fluctuations has been discussed in great detail (e.g., Barron et al. 1985; Eicher and Diner 1985; Sageman et al. 1997; Leckie et al. 1998; Elderbak and Leckie 2016; Jones et al. 2019) with a variety of interpretations of the significance of limestones in terms of productivity and dilution. The temporal significance of longer-term fluctuations in $\%CaCO_3$ have been discussed by Elder et al. (1994), Laurin and Sageman (2007), Elderbak and Leckie (2016) and Jones et al. (2019) who have demonstrated that the prominent limestone beds (LS1 to LS9 in text-figs 4 and 5) correlate across the WIS. These beds have been recognized as flooding surfaces (Elder et al. 1994). The moderately-strong correlation between $\%CaCO_3$ and the abundance of *W. barnesiae* and *C. margerelii* also suggests an environmental control with the peaks in $\%CaCO_3$ correlating to intervals of warming and concomitant intensified surface ocean stratification. Elderbak and Leckie (2016) interpreted limestone intervals as times of elevated productivity, and, as discussed, this is not inconsistent with the interpretation of nannoplankton assemblages. It is possible that stratification and increased productivity were linked via increased runoff from the adjacent continental margin during warm and wet intervals, but this hypothesis needs more testing.

Although the changes observed at SH#1 are among the most pronounced, they mirror assemblage shifts elsewhere. Burns and Bralower (1998), Eleson and Bralower (2005) and Corbett and Watkins (2013) observed decreases in the abundance of *B. constans* during the core of OAE2 in Texas, Kansas and Colorado (text-fig. 9). In fact, the decrease in the abundance of *B. constans* may have been a super-regional or even a global event (e.g., Erba 2004).

Both Watkins (1986) and Corbett and Watkins (2013) proposed that the core of OAE2 was stratified in the WIS as a result of the superposition of fresher Boreal waters over Tethyan waters. The changes in the warm and stratification marker taxa, particularly *Eprolithus* spp., *W. barnesiae*, and *C. margerelii,* are more pronounced than at sites from the central part of the seaway and we speculate that stratification was at least partially a response to warming during the height of OAE2, when it was significant enough to transform the whole nannoplankton assemblage. However, it is clear that stratification was not just a regional WIS occurrence. *Eprolithus* spp. blooms have been observed at other Cenomanian–Turonian WIS locations (Bralower 1988) and boundary sites from northern Europe and Africa (Lamolda et al. 1994; Tantawy 2008; Melinte-Dobrinescu and Bojar 2008; Hardas et al. 2012; Linnert and Mutterlose 2015) showing that it was in fact an oceanwide occurrence during OAE2, even though paleoecological interpretations differ (Table 4). Thus, stratification likely played a significant role in organic carbon burial along with increased organic productivity.

CONCLUSIONS

The Tropic Shale in the SH#1 core contains well-preserved calcareous nannofossil assemblages that illustrate significant changes in oceanographic conditions and the paleoecology of nanoplankton during OAE2. Our detailed assemblage study is designed to interpret the ecology of taxa as well as the significance of their changes. Cluster analysis and DCA support previous paleoecological interpretations including *B. constans* as a cool and eutrophic species and *W. barnesiae* as a warm water indicator. These analyses also help refine the paleoecological/paleoceanographic affinities of other taxa: *C. margerelii, E. floralis*, and *E. moratus* appear to have an affinity for stratified water masses.

Trace element concentrations show broad correlation with the positive carbon isotope excursion confirming the link between volcanism and productivity on a global scale. However, there is no correlation between trace metal concentrations and the abundances of individual calcareous nannofossil taxa in the SH#1 core. Assemblages, specifically the abundance of *B. constans*, document pulses of eutrophic, Boreal waters along the western margin of the WIS; the first pulse occurred at the beginning of OAE2 and the second at the end of OAE2. The decrease in the abundance of *Biscutum constans* at the onset of OAE2 and short peaks in the abundance of *Eprolithus* spp. during it are super regional or possibly global in extent. However, the assemblages, specifically the abundance of *W. barnesiae*, indicate that location of SH#1 during the core of OAE2 was bathed by warm and stratified surface waters, a pattern documented from other sites in the WIS. Cyclicity in percent abundance of *W. barnesiae* and *C. margerelii* show moderately strong correlation with $\%CaCO_3$ and this suggests a relationship between warming and intensified surface ocean stratification. Increased stratification is a surface ocean trademark of warming during OAE2 and may have driven increased productivity over large areas of the ocean and been instrumental in the deposition of organic-rich sediments.

Data Availability

Nannofossil assemblage and trace element data are available on the Pangaea Data Publisher at:
https://doi.pangaea.de/10.1594/PANGAEA.938507.

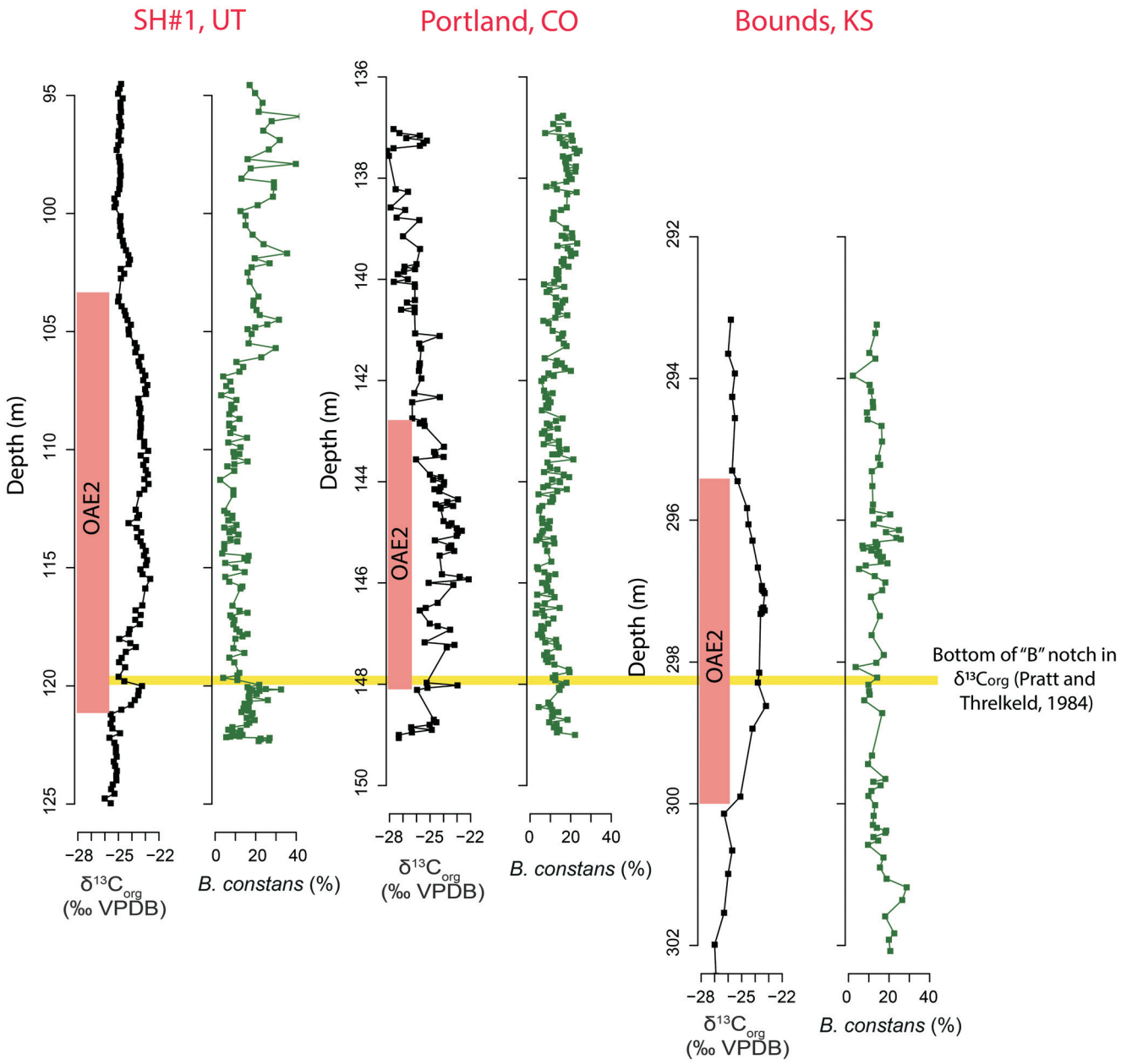

TEXT-FIGURE 9
Comparison of the relative abundance of *B. constans* for the SH#1, Portland (PO) and Bounds (BO) cores across the Cenomanian/Turonian Boundary during OAE2. PO and BO data are from Burns and Bralower (1998). Sections have been correlated in time using the "B" interval of the organic carbon isotope excursion as defined by (Pratt 1985).

ACKNOWLEDGMENTS

We thank Matt Fantle, Lee Kump, Mike Arthur, and Mark Patzkowsky for discussions that helped shape our interpretations. We thank Jason Parlett and the USGS Denver drilling team for the superb coring at Smoky Hollow, Chris Lowery, Scott Karduck and Lindsey Victoria for help in the field and Matt Gonzalez and Scott Karduck for help in the laboratory. We are grateful to Elisabetta Erba, Jean Self-Trail, and David Watkins for extremely helpful reviews. We gratefully acknowledge funding from the National Science Foundation (EAR-1338316) and the late Rich Lane for his instrumental role in initiating the Earth-Life Transitions program.

REFERENCES

ADAMS, D. D., HURTGEN, M. T. and SAGEMAN, B. B., 2010. Volcanic triggering of a biogeochemical cascade during Oceanic Anoxic Event 2. *Nature Geoscience,* 3: 201–204.

ARTHUR, M. and SAGEMAN, B., 1994. Marine black shales: A review of depositional mechanisms and environments of ancient deposits. *Annual Review Earth and Planetary Sciences*, 22: 499–551.

ARTHUR, M., SCHLANGER, S., JENKYNS, H., BROOKS, J. and FLEET, A., 1987. Marine Petroleum Source Rocks. *Geological Society Special Publication,* 26: 401–420.

ARTHUR, M. A., DEAN, W. E. and SCHLANGER, S., 1985. Variations in the global carbon cycle during the Cretaceous related to climate, volcanism, and changes in atmospheric CO2. In Sundquist, E. T. and Broecker, W. S., Eds., *The carbon cycle and atmospheric CO2: Natural variations Archean to present,* American Geophysical Union, 32: 504–529.

ARTHUR, M. A. and SAGEMAN, B. B., 2005. Sea-level control on source-rock development: perspectives from the Holocene Black Sea, the mid-Cretaceous Western Interior Basin of North America, and the Late Devonian Appalachian Basin. In: Harris, N. B., Ed., *The Deposition of Organic Carbon Rich Sediments: Models, Mechanisms and Consequences*. Society of Economic Paleontologists and Mineralogists Special Publication, 82: 35–59.

BARCLAY, R. S., MCELWAIN, J. C. and SAGEMAN, B. B., 2010. Carbon sequestration activated by a volcanic CO 2 pulse during Ocean Anoxic Event 2. *Nature Geoscience,* 3: 205–208.

BARRON, E. J., ARTHUR, M. A. and KAUFFMAN, E. G., 1985. Cretaceous rhythmic bedding sequences: a plausible link between orbital variations and climate. *Earth and Planetary Science Letters,* 72: 327–340.

BOTTINI, C. and ERBA, E., 2018. Mid-Cretaceous paleoenvironmental changes in the western Tethys. *Climate of the Past,* 14: 1147–1163.

BOTTINI, C. and FAUCHER, G., 2020. *Biscutum constans* coccolith size patterns across the mid Cretaceous in the western Tethys: Paleoecological implications. *Palaeogeography, Palaeoclimatology, Palaeoecology,* 555: 109852.

BOUDINOT, F. G., DILDAR, N., LECKIE, R. M., PARKER, A., JONES, M. M., SAGEMAN, B. B., BRALOWER, T. J. and SEPÚLVEDA, J., 2020. Neritic ecosystem response to Oceanic Anoxic Event 2 in the Cretaceous Western Interior Seaway, USA. *Palaeogeography, Palaeoclimatology, Palaeoecology,* 546: 109673.

BOUDINOT, F. G. and SEPÚLVEDA, J., 2020. Marine organic carbon burial increased forest fire frequency during Oceanic Anoxic Event 2. *Nature Geoscience,* 13: 693–698.

BRALOWER, T. J., 1988. Calcareous nannofossil biostratigraphy and assemblages of the Cenomanian Turonian boundary interval: Implications for the origin and timing of oceanic anoxia. *Paleoceanography,* 3: 275–316.

BRALOWER, T. J. and BERGEN, J. A., 1998. Cenomanian-Santonian calcareous nannofossil biostratigraphy of a transect of cores drilled across the Western Interior Seaway. In: Arthur, M. A. and Dean, W. E., Eds., *The Cretaceous Western Interior Drilling Program.* Society of Economic Paleontologists and Mineralogists, Concepts in Sedimentology and Paleontology, 6: 15–35.

BRUMSACK, H.-J., 2006. The trace metal content of recent organic carbon-rich sediments: implications for Cretaceous black shale formation. *Palaeogeography, Palaeoclimatology, Palaeoecology,* 232: 344–361.

BRYANT, R., LECKIE, R. M., BRALOWER, T. J., JONES, M. M., SAGEMAN, B. B., 2021. Microfossil and geochemical records reveal unique paleoenvironments near the southwestern edge of the Western Interior Seaway during Oceanic Anoxic Event 2. *Palaeogeography, Palaeoclimatology, Palaeoecology,* 584: 110679.

BURNETT, J., GALLAGHER, L. and HAMPTON, M., 1998. Upper Cretaceous. In: Bown, P. R., Ed., *Calcareous nannofossil biostratigraphy.* London: Chapman and Hall, 132–199.

BURNS, C. E. and BRALOWER, T. J., 1998. Upper Cretaceous nannofossil assemblages across the Western Interior Seaway: implications for the origins of lithologic cycles in the Greenhorn and Niobrara Formations. In: Arthur, M. A. and Dean, W. E., Eds., *The Cretaceous Western Interior Drilling Program.* Society of Economic Paleontologists and Mineralogists, Concepts in Sedimentology and Paleontology, 6: 35–58.

CARPENTER, K., MACLEAN, J., BIEK, R. and HUNTOON, J., 2014. Where the sea meets the land—the unresolved Dakota problem in Utah. *Utah Geological Association Publication,* 43: 357–372.

CLARK, B., 2018. "Numerical simulations of productivity and anoxa in the Western Interior Seaway during Oceanic Anoxic Event 2 (93.9 Ma)". Unpublished M.S. Thesis, The Pennsylvania State University.

CORBETT, M. J. and WATKINS, D. K., 2013. Calcareous nannofossil paleoecology of the mid-Cretaceous Western Interior Seaway and evidence of oligotrophic surface waters during OAE2. *Palaeogeography, Palaeoclimatology, Palaeoecology,* 392: 510–523.

DAMSTÉ, J. S. S., KUYPERS, M. M., PANCOST, R. D. and SCHOUTEN, S., 2008. The carbon isotopic response of algae, (cyano) bacteria, archaea and higher plants to the late Cenomanian perturbation of the global carbon cycle: Insights from biomarkers in black shales from the Cape Verde Basin (DSDP Site 367). *Organic Geochemistry,* 39: 1703–1718.

DUMITRESCU, M. and BRASSELL, S. C., 2006. Compositional and isotopic characteristics of organic matter for the early Aptian Oceanic Anoxic Event at Shatsky Rise, ODP Leg 198. *Palaeogeography, Palaeoclimatology, Palaeoecology,* 235: 168–191.

EICHER, D. L. and DINER, R., 1985. Foraminifera as indicators of water mass in the Cretaceous Greenhorn Sea, Western Interior. In: Pratt, L. M., Kauffman, E. G. and Zelt, F. B., Eds., *Fine-grained deposits and biofacies of the Cretaceous Western Interior Seaway: Evidence of cyclic sedimentary processes*, *Society of Economic Paleontologists and Mineralogists Field Trip Guidebook*, 4: 60-71.

EICHER, D. L. and WORSTELL, P., 1970. Cenomanian and Turonian foraminifera from the great plains, United States. *Micropaleontology,* 16: 269–324.

ELDER, W. P., 1985. Biotic patterns across the Cenomanian-Turonian extinction boundary near Pueblo, Colorado. In: Pratt, L. M., Kauffman, E. G. and Zelt, F. B., Eds., *Fine-grained deposits and biofacies of the Cretaceous Western Interior Seaway: Evidence of cyclic sedimentary processes*, *Society of Economic Paleontologists and Mineralogists Field Trip Guidebook*, 4: 157–169.

———, 1989. Molluscan extinction patterns across the Cenomanian-Turonian stage boundary in the Western Interior of the United States. *Paleobiology,* 15: 299–320.

ELDER, W. P., GUSTASON, E. R. and SAGEMAN, B. B., 1994. Correlation of basinal carbonate cycles to nearshore parasequences in the Late Cretaceous Greenhorn seaway, Western Interior USA. *Geological Society of America Bulletin,* 106: 892–902.

ELDERBAK, K. and LECKIE, R. M., 2016. Paleocirculation and foraminiferal assemblages of the Cenomanian–Turonian Bridge Creek Limestone bedding couplets: Productivity vs. dilution during OAE2. *Cretaceous Research,* 60: 52–77.

ELESON, J. W. and BRALOWER, T. J., 2005. Evidence of changes in surface water temperature and productivity at the Cenomanian/Turonian Boundary. *Micropaleontology,* 51: 319–332.

ENGLEMAN, E. E., JACKSON, L. L. and NORTON, D. R., 1985. Determination of carbonate carbon in geological materials by coulometric titration. *Chemical Geology,* 53: 125–128.

ERBA, E., 2004. Calcareous nannofossils and Mesozoic oceanic anoxic events. *Marine Micropaleontology,* 52: 85–106.

ERBA, E., CASTRADORI, D., GUASTI, G. and RIPEPE, M., 1992. Calcareous nannofossils and Milankovitch cycles: the example of the Albian Gault Clay Formation (southern England). *Palaeogeography, Palaeoclimatology, Palaeoecology,* 93: 47–69.

ERBA, E., DUNCAN, R. A., BOTTINI, C., TIRABOSCHI, D., WEISSERT, H., JENKYNS, H. C. and MALINVERNO, A., 2015. Environmental consequences of Ontong Java Plateau and Kerguelen Plateau volcanism. *The origin, evolution, and environmental impact of oceanic large igneous provinces. Geological Society of America Special Paper,* 511: 271–303.

FAUCHER, G., HOFFMANN, L., BACH, L. T., BOTTINI, C., ERBA, E. and RIEBESELL, U., 2017. Impact of trace metal concentrations on coccolithophore growth and morphology: laboratory simulations of Cretaceous stress. *Biogeosciences,* 14: 3603–3613.

FORSTER, A., SCHOUTEN, S., BAAS, M. and SINNINGHE DAMSTÉ, J. S., 2007. Mid-Cretaceous (Albian–Santonian) sea surface temperature record of the tropical Atlantic Ocean. *Geology,* 35: 919–922.

FORTIZ, V., 2017. Oceanic Anoxic Event 2 (93.9 Ma) in the U.S. Western Interior Seaway: High-Resolution Caclareous Nannofossil Record of the Tropic Shale Formation. *Unpublished M.S. Thesis, The Pennsylvania State University.*

GALE, A. S., VOIGT, S., SAGEMAN, B. B. and KENNEDY, W. J., 2008. Eustatic sea-level record for the Cenomanian (Late Cretaceous)—extension to the Western Interior Basin, USA. *Geology,* 36: 859–862.

HALLOCK, P., 1987. Fluctuations in the trophic resource continuum: a factor in global diversity cycles? *Paleoceanography,* 2: 457–471.

HAQ, B. U., HARDENBOL, J. and VAIL, P. R., 1987. Chronology of fluctuating sea levels since the Triassic. *Science,* 235: 1156–1167.

HARDAS, P. and MUTTERLOSE, J., 2007. Calcareous nannofossil assemblages of Oceanic Anoxic Event 2 in the equatorial Atlantic: Evidence of an eutrophication event. *Marine Micropaleontology,* 66: 52–69.

HARDAS, P., MUTTERLOSE, J., FRIEDRICH, O. and ERBACHER, J., 2012. The Middle Cenomanian Event in the equatorial Atlantic: the calcareous nannofossil and benthic foraminiferal response. *Marine Micropaleontology,* 96: 66–74.

HARRIES, P. J. and LITTLE, C. T., 1999. The early Toarcian (Early Jurassic) and the Cenomanian–Turonian (Late Cretaceous) mass extinctions: similarities and contrasts. *Palaeogeography, Palaeoclimatology, Palaeoecology,* 154: 39–66.

HERRLE, J. O., PROSS, J., FRIEDRICH, O., KÖSSLE, P. and HEMLEBEN, C., 2003. Forcing mechanisms for mid-Cretaceous black shale formation: evidence from the Upper Aptian and Lower Albian of the Vocontian Basin (SE France). *Palaeogeography, Palaeoclimatology, Palaeoecology,* 190: 399–426.

HILL, M., 1975. Selective dissolution of mid-Cretaceous (Cenomanian) calcareous nannofossils. *Micropaleontology,* 21: 227–235.

HOLMDEN, C., JACOBSON, A., SAGEMAN, B. and HURTGEN, M., 2016. Response of the Cr isotope proxy to Cretaceous Ocean Anoxic Event 2 in a pelagic carbonate succession from the Western Interior Seaway. *Geochimica et Cosmochimica Acta,* 186: 277–295.

HUBER, B. T., NORRIS, R. D. and MACLEOD, K. G., 2002. Deep-sea paleotemperature record of extreme warmth during the Cretaceous. *Geology,* 30: 123–126.

JENKYNS, H., 1980. Cretaceous anoxic events: from continents to oceans. *Journal of the Geological Society,* 137: 171–188.

JENKYNS, H. C., 2010. Geochemistry of oceanic anoxic events. *Geochemistry, Geophysics, Geosystems,* 11: 1–30.

———, 2018. Transient cooling episodes during Cretaceous Oceanic Anoxic Events with special reference to OAE 1a (Early Aptian). *Philosophical Transactions of the Royal Society A: Mathematical, Physical and Engineering Sciences,* 376: 20170073.

JONES, M. M., SAGEMAN, B. B., OAKES, R. L., PARKER, A. L., LECKIE, R. M., BRALOWER, T. J., SEPÚLVEDA, J. and FORTIZ, V., 2019. Astronomical pacing of relative sea level during Oceanic Anoxic Event 2: Preliminary studies of the expanded SH# 1 Core, Utah, USA. *Geological Society of America Bulletin,* 131: 1702–1722.

JONES, M. M., SAGEMAN, B. B., SELBY, D., JICHA, B. R., SINGER, B. S. and TITUS, A. L., 2021. Regional chronostratigraphic synthesis of the Cenomanian-Turonian Oceanic Anoxic Event 2 (OAE2) interval, Western Interior Basin (USA): New Re-Os chemostratigraphy and 40Ar/39Ar geochronology. *Geological Society of America Bulletin,* 133: 1090–1104.

KAUFFMAN, E. G., 1977. Geological and biological overview: Western Interior Cretaceous basin. *The Mountain Geologist*, 14: 255–274.

———, 1984. Paleobiogeography and evolutionary response dynamic in the Cretaceous Western Interior Seaway of North America. *Jurassic-Cretaceous biochronology and paleogeography of North America.* Geological Association of Canada Special Paper, 27: 273–306.

KERR, A. C., 1998. Oceanic plateau formation: a cause of mass extinction and black shale deposition around the Cenomanian–Turonian boundary? *Journal of the Geological Society,* 155: 619–626.

LAMOLDA, M., GOROSTIDI, A. and PAUL, C., 1994. Quantitative estimates of calcareous nannofossil changes across the Plenus Marls (latest Cenomanian), Dover, England: implications for the generation of the Cenomanian-Turonian Boundary Event. *Cretaceous Research,* 15: 143–164.

LARSON, R. L. 1991. Geological consequences of superplumes. *Geology,* 19: 963–966.

LAURIN, J., BARCLAY, R. S., SAGEMAN, B. B., DAWSON, R. R., PAGANI, M., SCHMITZ, M., EATON, J., MCINERNEY, F. A. and MCELWAIN, J. C., 2019. Terrestrial and marginal-marine record of the mid-Cretaceous Oceanic Anoxic Event 2 (OAE 2): High-resolution framework, carbon isotopes, CO2 and sea-level change. *Palaeogeography, Palaeoclimatology, Palaeoecology,* 524: 118–136.

LAURIN, J. and SAGEMAN, B. B., 2007. Cenomanian–Turonian coastal record in SW Utah, USA: Orbital-scale transgressive–regressive events during Oceanic Anoxic Event II. *Journal of Sedimentary Research,* 77: 731–756.

LECKIE, R. M., 1985. Foraninifera of the Cenomanian-Turonian Boundary Interval, Greenhorn Formation, Rock Canyon Anticline, Pueblo, Colorado. In: Pratt, L. M., Kauffman, E. G. and Zelt F. B., Eds., *Fine-grained deposits and biofacies of the Cretaceous Western Interior Seaway: Evidence of cyclic sedimentary processes*. Society of Economic Paleontologists and Mineralogists Field Trip Guidebook, 4: 139–150.

LECKIE, R. M., BRALOWER, T. J. and CASHMAN, R., 2002. Oceanic anoxic events and plankton evolution: Biotic response to tectonic forcing during the mid Cretaceous. *Paleoceanography,* 17 (3): 13-1–13-29.

LECKIE, R. M., SCHMIDT, M. G., FINKELSTEIN, D., YURETICH, R., NATIONS, J. D. and EATON, J. G., 1991. Paleoceanographic and paleoclimatic interpretations of the Mancos Shale (Upper Cretaceous), Black Mesa Basin, Arizona. In: Nations, J. D. and Eaton, J. G., Eds., *Stratigraphy, Depositional Environments, and Sedimentary Tectonics of the Western Margin, Cretaceous Western Interior Seaway.* Geological Society of America Special Paper, 260: 139–152.

LECKIE, R. M., YURETICH, R. F., WEST, O. L., FINKELSTEIN, D. and SCHMIDT, M., 1998. Paleoceanography of the southwestern Western Interior Sea during the time of the Cenomanian-Turonian boundary (Late Cretaceous). In: Dean, W. E. and Arthur, M. A., Eds., *Stratigraphy and Paleoenvironments of the Western Interior Seaway, USA, Concepts in Sedimentology and Paleontology no.6.* Society for Sedimentary Geology, 101–126.

LEES, J. A., 2002. Calcareous nannofossil biogeography illustrates palaeoclimate change in the Late Cretaceous Indian Ocean. *Cretaceous Research,* 23: 537–634.

LEES, J. A., BOWN, P. R., YOUNG, J. R. and RIDING, J. B., 2004. Evidence for annual records of phytoplankton productivity in the Kimmeridge Clay Formation coccolith stone bands (Upper Jurassic, Dorset, UK). *Marine Micropaleontology,* 52: 29–49.

LEITHOLD, E. L., 1993. Preservation of laminated shale in ancient clinoforms; comparison to modern subaqueous deltas. *Geology,* 21: 359–362.

———, 1994. Stratigraphical architecture at the muddy margin of the Cretaceous Western Interior Seaway, southern Utah. *Sedimentology,* 41: 521–542.

LINNERT, C. and MUTTERLOSE, J., 2015. Boreal early Turonian calcareous nannofossils from nearshore settings—implications for Paleoecology. *Palaios,* 30: 728–742.

LOWERY, C. M., CORBETT, M. J., LECKIE, R. M., WATKINS, D., ROMERO, A. M. and PRAMUDITO, A. 2014. Foraminiferal and nannofossil paleoecology and paleoceanography of the Cenomanian–Turonian Eagle Ford Shale of southern Texas. *Palaeogeography, Palaeoclimatology, Palaeoecology,* 413: 49–65.

LOWERY, C. M., LECKIE, R. M., BRYANT, R., ELDERBAK, K., PARKER, A., POLYAK, D. E., SCHMIDT, M., SNOEYENBOS-WEST, O. and STERZINAR, E., 2018. The Late Cretaceous Western Interior Seaway as a model for oxygenation change in epicontinental restricted basins. *Earth-Science Reviews,* 177: 545–564.

LOWERY, C. M., SELF-TRAIL, J. M. and BARRIE, C. D., 2021. Enhanced terrestrial runoff during Oceanic Anoxic Event 2 on the North Carolina Coastal Plain, USA. *Climate of the Past,* 17: 1227–1242.

MAECHLER, M., ROUSSEEUW, P., STRUYF, A., HUBERT, M., HORNIK, K. and STUDER, M., 2013. Package 'cluster'. *Dosegljivo na*.

MCCABE, P. J. and PARRISH, J. T., 1992. *Controls on the distribution and quality of Cretaceous coals*, *Special Paper Geological Society of America*, 267: 1–15.

MCCUNE, B., GRACE, J. B. and URBAN, D. L., 2002. *Analysis of ecological communities*, MjM software design, Gleneden Beach, OR.

MCKEAN, R. L. S. and GILLETTE, D. D., 2015. Taphonomy of large marine vertebrates in the Upper Cretaceous (Cenomanian-Turonian) tropic shale of southern Utah. *Cretaceous Research,* 56: 278–292.

MELINTE-DOBRINESCU, M. C. and BOJAR, A.-V., 2008. Biostratigraphic and isotopic record of the Cenomanian–Turonian deposits in the Ohaba-Ponor section (SW Haţeg, Romania) *Cretaceous Research,* 29: 1024–1034.

MEYERS, S. R., 2007. Production and preservation of organic matter: The significance of iron. *Paleoceanography,* 22.

MEYERS, S. R., SAGEMAN, B. B. and LYONS, T. W., 2005. Organic carbon burial rate and the molybdenum proxy: Theoretical framework and application to Cenomanian Turonian oceanic anoxic event 2. *Paleoceanography,* 20.

MEYERS, S. R., SIEWERT, S. E., SINGER, B. S., SAGEMAN, B. B., CONDON, D. J., OBRADOVICH, J. D., JICHA, B. R. and SAWYER, D. A., 2012. Intercalibration of radioisotopic and astrochronologic time scales for the Cenomanian-Turonian boundary interval, Western Interior Basin, USA. *Geology,* 40: 7–10.

MONECHI, S. and THIERSTEIN, H. R., 1985. Late Cretaceous-Eocene nannofossil and magnetostratigraphic correlations near Gubbio, Italy. *Marine Micropaleontology,* 9: 419–440.

MORT, H. P., ADATTE, T., FO¨LLMI, K. B., KELLER, G., STEINMANN, P., MATERA, V., BERNER, Z. and STÜBEN, D., 2007. Phosphorus and the roles of productivity and nutrient recycling during oceanic anoxic event 2. *Geology,* 35: 483–486.

MUTTERLOSE, J. and KESSELS, K., 2000. Early Cretaceous calcareous nannofossils from high latitudes: implications for palaeobiogeography and palaeoclimate. *Palaeogeography, Palaeoclimatology, Palaeoecology,* 160: 347–372.

O'CONNOR, L. K., JENKYNS, H. C., ROBINSON, S. A., REMMELZWAAL, S. R., BATENBURG, S. J., PARKINSON, I. J. and GALE, A. S., 2020. A re evaluation of the Plenus Cold Event, and the links between CO2, temperature, and seawater chemistry during OAE 2. *Paleoceanography and Paleoclimatology,* 35:e2019PA003631.

OKSANEN, J., BLANCHET, F., FRIENDLY, M., KINDT, R., LEGENDRE, P., MCGLINN, D., MINCHIN, P., O'HARA, R., SIMPSON, G. and SOLYMOS, P., 2019. vegan: Community Ecology Package. 2019. R package version 2.5-6.

ORTH, C. J., ATTREP JR, M., QUINTANA, L. R., ELDER, W. P., KAUFFMAN, E. G., DINER, R. and VILLAMIL, T., 1993. Elemental abundance anomalies in the late Cenomanian extinction interval: a search for the source (s). *Earth and Planetary Science Letters,* 117: 189–204.

PERCH-NIELSEN, K., BOLLI, H. and SAUNDERS, J., 1985. Mesozoic calcareous nannofossils. In: Bolli, H. M., Saunders, J. B. and Perch-Nielsen, K., Eds., *Plankton Stratigraphy,* Cambridge: Cambridge University Press, 329–426.

PRATT, L. M., 1985. Isotopic studies of organic matter and carbonate in rocks of the Greenhorn marine cycle. In: Pratt, L. M., Kauffman, E. G. and Zelt, F. B., Eds., *Fine-grained deposits and biofacies of the Cretaceous Western Interior Seaway: Evidence of cyclic sedimentary processes*. Society of Economic Paleontologists and Mineralogists Field Trip Guidebook, 4: 38–48.

RAUP, D. M. and SEPKOSKI, J. J., 1982. Mass extinctions in the marine fossil record. *Science,* 215: 1501–1503.

ROBINSON, S. A., HEIMHOFER, U., HESSELBO, S. P. and PETRIZZO, M. R., 2017. Mesozoic climates and oceans–a tribute to Hugh Jenkyns and Helmut Weissert. *Sedimentology,* 64: 1–15.

ROTH, P. H., 1981. Mid-Cretaceous calcareous nannoplankton from the Central Pacific; implications for paleoceanography. *Initial Reports Deep Sea Drilling Project*, 62: 471–489.

———, 1989. Ocean circulation and calcareous nannoplankton evolution during the Jurassic and Cretaceous. *Palaeogeography, Palaeoclimatology, Palaeoecology,* 74: 111–126.

ROTH, P. H. and BOWDLER, J. L., 1981. Middle Cretaceous calcareous nannoplankton biogeography and oceanography of the Atlantic Ocean. In: Warme, J. E., Douglas, R. G. and Winterer, E. L., Eds., *The Deep Sea Drilling Project: A Decade of Progress*. Society of Economic Paleontologists and Mineralogists Special Publication, 32: 517-546.

ROTH, P. H. and KRUMBACH, K. R., 1986. Middle Cretaceous calcareous nannofossil biogeography and preservation in the Atlantic and Indian Oceans: implications for paleoceanography. *Marine Micropaleontology,* 10: 235–266.

RUBIN, K., 1997. Degassing of metals and metalloids from erupting seamount and mid-ocean ridge volcanoes: Observations and predictions. *Geochimica et Cosmochimica Acta,* 61: 3525–3542.

SAGEMAN, B. B., MEYERS, S. R. and ARTHUR, M. A., 2006. Orbital time scale and new C-isotope record for Cenomanian-Turonian boundary stratotype. *Geology,* 34: 125–128.

SAGEMAN, B. B., RICH, J., ARTHUR, M. A., BIRCHFIELD, G. and DEAN, W., 1997. Evidence for Milankovitch periodicities in Cenomanian-Turonian lithologic and geochemical cycles, Western Interior USA. *Journal of Sedimentary Research,* 67: 286–302.

SCHLANGER, S., ARTHUR, M., JENKYNS, H. and SCHOLLE, P., 1987. The Cenomanian-Turonian Oceanic Anoxic Event, I. Stratigraphy and distribution of organic carbon-rich beds and the marine $\delta^{13}C$ excursion. *Geological Society, London, Special Publications,* 26: 371–399.

SCHLANGER, S. and JENKYNS, H., 1976. Cretaceous oceanic anoxic events: Causes and consequences. *Geologie en Mijnbouw,* 55 (3-4): 179–184.

SCHOLLE, P. A. and ARTHUR, M. A., 1980. Carbon isotope fluctuations in Cretaceous pelagic limestones: potential stratigraphic and petroleum exploration tool. *AAPG Bulletin,* 64: 67–87.

SETON, M., GAINA, C., MÜLLER, R. and HEINE, C., 2009. Mid-Cretaceous seafloor spreading pulse: Fact or fiction? *Geology,* 37: 687–690.

SILVÁ, I. P., ERBA, E. and TORNAGHI, M. E., 1989. Paleoenvironmental signals and changes in surface fertilityin Mid Cretaceous Corg-Rich pelagic facies of the Fucoid Marls (Central Italy). *Geobios,* 22: 225–236.

SLINGERLAND, R., KUMP, L. R., ARTHUR, M. A., FAWCETT, P. J., SAGEMAN, B. B. and BARRON, E. J., 1996. Estuarine circulation in the Turonian western interior seaway of North America. *Geological Society of America Bulletin,* 108: 941–952.

SNOW, L. J., DUNCAN, R. A. and BRALOWER, T. J., 2005. Trace element abundances in the Rock Canyon Anticline, Pueblo, Colorado, marine sedimentary section and their relationship to Caribbean plateau construction and oxygen anoxic event 2. *Paleoceanography,* 20.

TANTAWY, A. A., 2008. Calcareous nannofossil biostratigraphy and paleoecology of the Cenomanian–Turonian transition in the Tarfaya Basin, southern Morocco. *Cretaceous Research,* 29: 995–1007.

THIERSTEIN, H., 1980. Selective dissolution of Late Cretaceous and earliest Tertiary calcareous nannofossils: experimental evidence. *Cretaceous Research,* 1: 165–176.

———, 1981. Late Cretaceous nannoplankton and the change at the Cretaceous Tertiary boundary. In: Warme, J.E., Winterer, E. and Douglas, R.G., Eds., *The Deep Sea Drilling Project: a decade of progress*. Society of Economic Paleontologists and Mineralogists, Special Publications, 32, 355–394.

THIERSTEIN, H. R. and ROTH, P. H., 1991. Stable isotopic and carbonate cyclicity in Lower Cretaceous deep-sea sediments: dominance of diagenetic effects. *Marine Geology,* 97: 1–34.

TIBERT, N. E., LECKIE, R. M., EATON, J. G., KIRKLAND, J. I., COLIN, J.-P., LEITHOLD, E. L. and MCCORMIC, M. E., 2003. Recognition of relative sea-level change in Upper Cretaceous coal-bearing strata: A paleoecological approach using agglutinated foraminifera and ostracodes to detect key stratigraphic surfaces. In: Olsen, H. C. and Leckie, R. M., Eds., *Micropaleontologic Proxies for Sea-Level Change and Stratigraphic Discontinuities*. Society of Economic Paleontologists and Mineralogists Special Publication, 75: 263–299.

TIRABOSCHI, D., ERBA, E. and JENKYNS, H. C., 2009. Origin of rhythmic Albian black shales (Piobbico core, central Italy): Calcareous nannofossil quantitative and statistical analyses and paleoceanographic reconstructions. *Paleoceanography,* 24.

TURGEON, S. C. and CREASER, R. A., 2008. Cretaceous oceanic anoxic event 2 triggered by a massive magmatic episode. *Nature,* 454: 323–326.

ULIČNÝ, D., 1999. Sequence stratigraphy of the Dakota Formation (Cenomanian), southern Utah: interplay of eustasy and tectonics in a foreland basin. *Sedimentology,* 46: 807–836.

VAN HELMOND, N. A., SLUIJS, A., REICHART, G.-J., SINNINGHE DAMSTÉ, J. S., SLOMP, C. P. and BRINKHUIS, H., 2014. A per-

turbed hydrological cycle during Oceanic Anoxic Event 2. *Geology,* 42: 123–126.

WATKINS, D., BRALOWER, T. J., COVINGTON, J. M. and FISHER, C. G., 1993. Biostratigraphy and paleoecology of the Upper Cretaceous calcareous nannofossils in the Western Interior Basin, North America. *Geological Association of Canada Special Paper,* 39: 521–537.

WATKINS, D. K., 1985. Biostratigraphy and paleoecology of calcareous nannofossils in the Greenhorn marine cycle. In: Pratt, L. M., Kauffman, E. G. and Zelt, F. B., Eds., *Fine-grained deposits and biofacies of the Cretaceous Western Interior Seaway: Evidence of cyclic sedimentary processes*, Society of Economic Paleontologists and Mineralogists Field Trip Guidebook, 4: 151–156.

———, 1986. Calcareous nannofossil paleoceanography of the Cretaceous Greenhorn Sea. *Geological Society of America Bulletin,* 97: 1239–1249.

———, 1989. Nannoplankton productivity fluctuations and rhythmically-bedded pelagic carbonates of the Greenhorn Limestone (Upper Cretaceous). *Palaeogeography, Palaeoclimatology, Palaeoecology,* 74: 75–86.

WILLIAMS, J. R. and BRALOWER, T. J., 1995. Nannofossil assemblages, fine fraction stable isotopes, and the paleoceanography of the Valanginian Barremian (early Cretaceous) North Sea Basin. *Paleoceanography,* 10: 815–839.

WITTEN, D. M. and TIBSHIRANI, R., 2010. A framework for feature selection in clustering. *Journal of the American Statistical Association,* 105: 713–726.

YOUNG, R. G. 1960. Dakota group of Colorado plateau. *AAPG Bulletin,* 44: 156–194.

ZENG, Z., PIKE, M., TICE, M. M., KELLY, C., MARCANTONIO, F., XU, G. and MAULANA, I., 2018. Iron fertilization of primary productivity by volcanic ash in the Late Cretaceous (Cenomanian) Western Interior Seaway. *Geology,* 46: 859–862.

ZIEGLER, A., RAYMOND, A., GIERLOWSKI, T., HORRELL, M., ROWLEY, D. and LOTTES, A., 1987. Coal, climate and terrestrial productivity: the present and early Cretaceous compared. *Geological Society, London, Special Publications,* 32: 25–49.

APPENDIX 1
List of nannofossil taxa

Axopodorhabdus albianus (Black 1967) Wind and Wise 1983
Biscutum constans (Górka 1957) Black *in* Black and Barnes 1959
Broinsonia enormis (Shumenko 1968) Manivit 1971
Broinsonia signata (Noël 1969) Noël 1970
Chiastozygus litterarius (Górka 1957) Manivit 1971
Chiastozygus spp. Gartner 1968
Corollithion achylosum (Stover 1966) Thierstein 1971
Corollithion signum Stradner 1963
Cretarhabdus angustiforatus Black 1971 Bukry 1973 emend. Bralower et al. 1989
Cretarhabdus conicus Bramlette and Martini 1964
Cretarhabdus coronadventis Reinhardt 1966
Cretarhabdus loriei Gartner 1968
Cretarhabdus surirellus (Deflandre and Fert 1954) Reinhardt 1970
Cribrosphaerella ehrenbergii (Arkhangelsky 1912) Deflandre in Piveteau 1952
Cyclagelosphaera margerelii Noël 1965
Eiffellithus turriseiffelii (Deflandre *in* Deflandre and Fert 1954) Reinhardt 1965
Eprolithus floralis (Stradner 1962) Stover 1966
Eprolithus moratus (Stover 1966) Burnett 1998
Flabellites oblongus (Bukry 1969) Crux *in* Crux et al. 1982
Gartnerago segmentatum (Stover 1966) Thierstein 1974
Grantarhabdus coronadventis (Reinhardt 1966) Grün *in* Grün and Allemann 1975
*Helenea chiastia*Worsley 1971
Helicolithus trabeculatus (Górka 1957) Verbeek 1977
Lithraphidites carniolensis Deflandre 1963
Manivitella pemmatoidea(Deflandre *in* Manivit 1965) Thierstein 1971
Markalius (Haquis) circumradiatus (Stover 1966) Roth 1978
Microrhabdulus decorates Deflandre 1959
Prediscosphaera cretacea (Arkhangelsky 1912) Gartner 1968
Prediscosphaera spinosa (Bramlette and Martini 1964) Gartner 1968
Quadrum gartneri Prins and Perch-Nielsen *in* Manivit et al. 197
Radiolithus planus Stover 1966
Rhagodiscus achlyostaurion (Hill 1976) Doeven 1983
Rhagodiscus angustus (Stradner 1963) Reinhardt 1971
Rhagodiscus asper (Stradner 1963) Reinhardt 1967
Rhagodiscus splendens (Deflandre 1953) Verbeek 1977
Rotellapillus laffittei Noël 1957
Scapholithus fossilis Deflandre in Deflandre and Fert 1954
Sollasites horticus (Stradner et al. *in* Stradner and Adamiker 1966) Cepek and Hay 1969
Tetrapodorhabdus decorus (Deflandre *in* Deflandre and Fert 1954) Wind and Wise 1983
Tranolithus gabalus Stover 1966
Tranolithus orionatus (Reinhardt 1966a) Reinhardt 1966b
Vagalapilla octoradiata (Górka 1957) Reinhardt 1966
Vagalapilla sp. Bukry 1969
Watznaueria barnesiae (Black *in* Black and Barnes 1959) Perch-Nielsen 1968
Watznaueria ovata Bukry 1969
Zeugrhabdotus embergeri (Deflandre *in* Deflandre and Fert 1954) Burnett *in* Gale et al. 1996
Zeugrhabdotus diplogrammus (Deflandre *in* Deflandre and Fert 1954) Burnett *in* Gale et al. 1996
Zeugrhabdotus elegans Gartner 1968
Zeugrhabdotus spiralis Bramlette and Martini 1964
Zeugrhabdotus erectus (Deflandre *in* Deflandre and Fert 1954) Reinhardt 1965